RESEARCH ARTICLE

Active photosynthetic inhibition mediated by MPK3/MPK6 is critical to effector-triggered immunity

Jianbin Su[1,2], Liuyi Yang[1], Qiankun Zhu[1], Hongjiao Wu[1], Yi He[1], Yidong Liu[2], Juan Xu[1], Dean Jiang[1], Shuqun Zhang[2]*

1 Key Laboratory of Plant Physiology and Biochemistry, College of Life Sciences, Zhejiang University, Hangzhou, Zhejiang, China, 2 Division of Biochemistry, Interdisciplinary Plant Group, and Bond Life Sciences Center, University of Missouri, Columbia, Missouri, United States of America

* zhangsh@missouri.edu

Abstract

Extensive research revealed tremendous details about how plants sense pathogen effectors during effector-triggered immunity (ETI). However, less is known about downstream signaling events. In this report, we demonstrate that prolonged activation of MPK3 and MPK6, two *Arabidopsis* pathogen-responsive mitogen-activated protein kinases (MPKs), is essential to ETI mediated by both coiled coil-nucleotide binding site-leucine rich repeats (CNLs) and toll/interleukin-1 receptor nucleotide binding site-leucine rich repeats (TNLs) types of R proteins. MPK3/MPK6 activation rapidly alters the expression of photosynthesis-related genes and inhibits photosynthesis, which promotes the accumulation of superoxide ($O_2^{\bullet-}$) and hydrogen peroxide (H_2O_2), two major reactive oxygen species (ROS), in chloroplasts under light. In the chemical-genetically rescued *mpk3 mpk6* double mutants, ETI-induced photosynthetic inhibition and chloroplastic ROS accumulation are compromised, which correlates with delayed hypersensitive response (HR) cell death and compromised resistance. Furthermore, protection of chloroplasts by expressing a plastid-targeted cyanobacterial flavodoxin (pFLD) delays photosynthetic inhibition and compromises ETI. Collectively, this study highlights a critical role of MPK3/MPK6 in manipulating plant photosynthetic activities to promote ROS accumulation in chloroplasts and HR cell death, which contributes to the robustness of ETI. Furthermore, the dual functionality of MPK3/MPK6 cascade in promoting defense and inhibiting photosynthesis potentially allow it to orchestrate the trade-off between plant growth and defense in plant immunity.

Author summary

Plants follow different strategies to defend themselves against pathogens and activate their immune systems once the pathogens have been detected. One of the responses observed is the inhibition of photosynthesis and the global down-regulation of genes that regulate this process, similar to what is frequently observed in plants under various biotic stress conditions. However, the mechanisms underlying the turning off of the photosynthetic activity

Abbreviations: *AvrB*, avirulence protein B; *AvrRpm1*, avirulence effector recognized by RPM1; *AvrRps4*, avirulence effector recognized by RPS4; *AvrRpt2*, avirulence effector recognized by RPS2; BN-PAGE, blue native-polyacrylamide gel electrophoresis; BR, brassinosteroid; CBB, Coomassie brilliant blue; CC, coiled-coil; CKI, cycline-dependent kinase inhibitor; CNL, coiled coil-nucleotide binding site-leucine rich repeat; Col-0, Columbia-0; CP43, photosystem II chlorophyll protein at 43 kDa; CRCK3, calmodulin binding receptor-like cytoplasmic kinase 3; DAB, 3,3'-diaminobenzidine; DAVID, Database for Annotation, Visualization and Integrated Discovery; *DD, GVG-NtMEK2^{DD}*; DEX, dexamethasone; dpi, days post inoculation; EDS1, Enhanced Disease Susceptibility 1; ETI, effector-triggered immunity; EtOH, ethanol; ETS, effector-triggered susceptibility; Fd, ferredoxin; FLAG, an octapeptide; Fld, flavodoxin; flg22, a 22 amino acids flagellin fragment; FLS2, flagellin-sensitive 2; FNR, ferredoxin-NADP$^+$ reductase; Fv/Fm, maximal PSII quantum yield; GA, gibberellic acid; GC, gas chromatography; GO, gene ontology; *GVG-AvrRpt2*, DEX-inducible promoter-driven *AvrRpt2*; H_2O_2, hydrogen peroxide; hpi, hours post inoculation; HR, hypersensitive response; *hrcC⁻*, mutant of outer membrane type III secretion protein HrcC; JA, jasmonic acid; LHCI, light-harvesting complex I; LHCII, light-harvesting complex II; LRR, leucine-rich repeat; MEKK2, MPK kinase kinase 2; MPK, mitogen-activated protein kinase; MS, Murashige and Skoog medium; NA-PP1, 4-amino-1-tert-butyl-3-(1'-naphthyl)pyrazolo[3,4-d]pyrimidine; NB-ARC, nucleotide binding site and ARC subdomain originating in Apaf1, R proteins, and CED-4; NBS, nucleotide binding site; NBT, nitroblue tetrazolium; NDH, NADH dehydrogenase-like; NLR, nucleotide-binding leucine-rich repeat R protein; NPQ, nonphotochemical quenching; NtMEK2, *Nicotiana tabacum* MAP kinase kinase 2; $O_2^{\bullet-}$, superoxide; OD, optical density; PAMP, pathogen/microbe-associated molecular pattern; *pBS, pBluescript*; *Pf0-1-AvrRpm1, P. fluorescens-AvrRpm1*; *Pf0-1-EV, P. fluorescens-EV*; pFld, plastid-targeted cyanobacterial flavodoxin; pMPK, phosphorylated MPK; PQ, plastoquinol; PRR, pattern recognition receptor; PSI, photosystem I;

and whether this process contributes to plants' defense against pathogens remain to be determined. In this study, we analyze these mechanisms in *Arabidopsis* plants and show that prolonged activation of MPK3 and MPK6, two kinases critical for pathogen resistance, results in the inhibition of photosynthesis and accumulation of reactive oxygen species (ROS) in the chloroplasts. We find that this response is similar to that observed during pathogen effector-triggered immunity (ETI). Correspondingly, plants that carry mutant versions of MPK3 and MPK6 result in compromised ETI-induced photosynthetic inhibition and chloroplastic ROS accumulation; thus, these two kinases seem to be essential for ETI. Our results suggest that MPK3/MPK6 activation induces a global down-regulation of photosynthesis along with an up-regulation of defense-related genes, and coordinates the growth and defense trade-off in plants.

Introduction

Plant defense against invading pathogens relies on a two-layered innate immune system. The first is the sensing of pathogen/microbe-associated molecular patterns (PAMPs) by plant pattern recognition receptors (PRRs), which induces a basal level resistance known as PAMP-triggered immunity (PTI) [1–5]. The second line of plant defense is activated by plant resistance (R) protein-mediated detection of pathogenic effectors, also known as effector-triggered immunity (ETI). The major feature of ETI is its robustness against pathogen infection, which is frequently associated with hypersensitive response (HR) cell death [1,3, 6–10].

All identified PRRs are membrane-localized receptor-like protein kinases (RLKs) or receptor-like proteins (RLPs) that detect conserved PAMPs such as bacterial flagellin and lipopolysaccharide or chitin from fungal cell walls [11,12]. Pathogen effectors are sensed by plant R proteins with diverse subcellular locations [13,14]. The majority of plant R proteins are nucleotide-binding site leucine-rich repeat (NBS-LRR) proteins, having a central NBS-ARC domain (ARC: Apaf1, R proteins, and CED-4) and a C-terminal leucine-rich repeat (LRR) domain [14–17]. Based on their N-terminal domains, plant NBS-LRR R proteins (NLRs) are classified into two families, the coiled coil-nucleotide binding site-leucine rich repeat (CNL) family and the Toll/interleukin-1 receptor-nucleotide binding site-leucine rich repeat (TNL) family [14–17]. Unlike PRRs, which detect PAMPs only by direct ligand-receptor recognition, NLRs utilize diverse strategies to detect effectors directly or indirectly. In the direct model, NLRs recognize their cognate effectors by direct protein–protein interactions, while the indirect recognition describes mechanisms by which NLRs sense effectors by monitoring modified self, including the "guard," the "decoy," and the "integrated decoy" model [18–20].

Compared to the well-studied effector recognition, the mechanisms underlying the activation of NLRs and their downstream signaling pathways are still poorly understood [14–17]. Current findings suggest that the activity of NLRs undergoes multilayered regulation, including self-inhibition, dimerization or oligomerization, epigenetic and transcriptional regulation, alternative splicing, and proteasome-mediated degradation [14–17]. Despite of the different recognition and activation mechanisms of NLRs and PRRs, ETI and PTI involve a similar set of downstream defense responses, including calcium-mediated signaling, activation of mitogen-activated protein kinases (MAPKs), production of reactive oxygen species (ROS), transcriptional reprogramming, and biosynthesis of antimicrobial compounds [3,4,7,21–28]. However, the responses during ETI have a longer duration and higher magnitude. As a result, ETI was proposed to be an amplified PTI [7]. Recently, it was proposed that plasma membrane–localized CNLs such as Resistance to *Pseudomonas syringae* pv *maculicola*

PSII, photosystem II; *Pst*, *Pseudomonas syringae* pv *tomato*; *Pst-EV*, *Pseudomonas syringae* pv. *tomato DC3000* carrying empty vector; pTEpY, dually phosphorylated Thr/Glu/Tyr peptide; PTI, PAMP-triggered immunity; PVDF, polyvinylidene fluoride; qPCR, quantitative PCR; RLCK, receptor-like cytoplasmic kinase; RLK, receptor-like protein kinase; RLP, receptor-like protein; RNA-seq, RNA sequencing; ROS, reactive oxygen species; RPM1, Resistance to *Pseudomonas syringae* pv *maculicola* 1; RPS2, Resistance to *Pseudomonas syringae* 2; RPS4, Resistance to *Pseudomonas syringae* 4; RPS6, Resistance to *Pseudomonas syringae* 6; RRS1, Resistance to *Ralstonia solanacearum* 1; RT-PCR, reverse transcription-polymerase chain reaction; SA, salicylic acid; SDS-PAGE, sodium dodecyl sulfate (SDS)-PAGE; SIPK, SA-induced protein kinase; SUMM2, suppressor of *mkk1 mkk2*; TIR, toll/interleukin-1 receptor; TNL, toll/interleukin-1 receptor-nucleotide binding site-leucine rich repeat; TTSS, type III secretion system; WIPK, wound-induced protein kinase; Y(II), PSII operating efficiency.

1 (RPM1), Resistance to *Pseudomonas syringae* 2 (RPS2), and Resistance to *Pseudomonas syringae* 5 (RPS5) trigger downstream defense responses similar to that activated by PRRs during PTI, with the exception of different magnitude and duration [12]. In contrast, ETI mediated by nucleus-localized TNLs, including Resistance to *Pseudomonas syringae* 4/Resistance to *Ralstonia solanacearum* 1 (RPS4/RRS1) and Resistance to *Pseudomonas syringae* 6 (RPS6), which is dependent on Enhanced Disease Susceptibility 1 (EDS1), seems to be more associated with transcriptional reprogramming [12]. This notion was supported by the findings that both plasma membrane–localized PRRs and CNL-type RPS2 can activate MPK3/MPK6 [24]. However, whether TNLs can activate MAPK signaling remains to be determined. Interestingly, EDS1 also contributes to RPS2-conditioned resistance when salicylic acid (SA) biosynthesis is blocked [29], indicating a complicated cross talk between CNL- and TNL-mediated resistance.

Recently, two new immune responses were identified, cell cycle repression and chloroplast stromule formation [30,31]. During ETI, the canonical function of cyclin-dependent kinase inhibitor (CKI)-retinoblastoma (RB)-E2F transcription factor in cell cycle progression is repressed and shifted to promote programmed cell death and transcriptional reprogramming [30]. Chloroplast stromules, dynamic tubular projections of chloroplasts, are strongly induced during plant immunity [31]. Some of the stromules were observed to connect chloroplasts with the nucleus, which was proposed to transport pro-defense signals, e.g., chloroplast-generated ROS, into the nucleus to promote transcriptional reprogramming [31]. At present, the mechanism underlying the generation of ROS in chloroplasts is still unclear. We have previously shown that prolonged activation of SA-induced protein kinase (SIPK) and wound-induced protein kinase (WIPK), the orthologs of *Arabidopsis* MPK6 and MPK3 in tobacco, respectively, inhibits photosynthesis and induces the accumulation of ROS in chloroplasts, which accelerates HR-like cell death in plants under light [32]. Later, chloroplast-originated ROS was implicated in promoting localized cell death in tobacco during nonhost interaction [33]. Because HR cell death can be uncoupled from ETI [34], i.e., host cell death is not the cause for resistance [7], it remains to be determined whether MAPK signaling and chloroplast-originated ROS accumulation contribute to ETI.

In *Arabidopsis*, MPK3, MPK6, MPK4, and MPK11 are rapidly activated during PTI and ETI [24,28,35]. They play critical roles in multiple plant defense responses, including activation of defense gene expression, induction of phytoalexin biosynthesis, and stomatal immunity [28,36–40]. Light is known to be critical to plant defense [41–43]. It has been known for decades that photosynthetic inhibition, including inhibition of photosystem II (PSII) activity, reduction of CO_2 fixation, and global down-regulation of photosynthetic genes, occurs after pathogen infection [44–50]. However, it is unclear whether the photosynthetic inhibition is a passive response due to pathogen infection or an active response regulated by host signaling pathways, i.e., whether photosynthetic inhibition is a part of plant immunity and contributes to plant disease resistance.

In this study, we demonstrate that both CNL and TNL NLR-mediated ETI induce prolonged activation of MPK3/MPK6, which contributes to the rapid and global inhibition of photosynthesis at multiple levels and the generation of ROS in chloroplasts. Loss-of-function of MPK3/MPK6 signaling compromises effector-triggered inhibition of photosynthetic activities, accumulation of ROS in chloroplasts, HR cell death, and pathogen resistance. Furthermore, it was discovered that inhibition of photosynthetic activities and chloroplastic ROS accumulation can mutually enhance each other. Based on these findings, we conclude that MPK3/MPK6-mediated active photosynthetic inhibition is a part of *Arabidopsis* immune response and plays a positive role during ETI.

Results

MPK3/MPK6 activation induces global down-regulation of genes related to photosynthesis

Inhibition of photosynthesis occurs in plants under a variety of abiotic and biotic stresses [44,51]. At present, it is unclear whether the inhibition is a passive response caused by stresses/pathogens or a response actively regulated by host signaling pathways, and if so, what the outcomes/functions are of such active inhibition. In our previous study, we found that activation of SIPK and WIPK, two stress-responsive MPKs in tobacco, causes rapid and strong inhibition of CO_2 fixation [32]. To elucidate the underlying mechanism, we utilized the *Arabidopsis* system and profiled the gene expression in the conditional gain-of-function *Arabidopsis GVG-NtMEK2^{DD}* (abbreviated as *DD*) transgenic plants. In this system, dexamethasone (DEX) treatment induces the expression of NtMEK2^{DD}, a constitutively active variant of *Nicotiana tabacum* MAP kinase kinase 2 (NtMEK2), which in turn activates specifically the endogenous MPK3 and MPK6 in *Arabidopsis* [52,53]. RNA sequencing (RNA-seq) profiling revealed a total of 2,984 genes that were down-regulated ($log_2 < −3$) and 1,042 genes up-regulated ($log_2 > 3$) at 6 h after DEX treatment (S1 Table). Genes involved in photosynthesis, including photosynthetic light harvesting, light reaction, electron transport, and dark reaction, were highly enriched in the down-regulated genes (Fig 1A and 1B). The up-regulated genes were mainly enriched in genes involved in plant–pathogen and plant–environment interactions and secondary metabolism (Fig 1C). Up-regulation of defense genes, including those involved in phytoalexin biosynthesis, is consistent with our previous reports [28,53–56]. Down-regulation of selected photosynthetic genes was further confirmed by quantitative reverse transcription-polymerase chain reaction (RT-PCR). As shown in Fig 1D, expression of genes involved in PSII repair (*LQY1* and *LTO1*), PSII assembly (*PAM68*), PSII stabilization (*PSB32*), and transcription in chloroplasts (e.g., *SIG1*–*SIG6*) were all decreased drastically after MPK3/MPK6 activation.

MPK3/MPK6 activation causes photosynthetic inhibition and ROS accumulation in chloroplasts

To determine the physiological consequences of the inhibition of photosynthetic genes, we measured PSII activity using chlorophyll fluorescence techniques [59]. As shown in Fig 2A and 2B, the maximal PSII activity parameter Fv/Fm and effective PSII operating efficiency parameter Y(II) both decreased upon MPK3/MPK6 activation. We next measured the fast chlorophyll fluorescence kinetics, also known as O-J-I-P curve [60]. The J-I rise was lower in DEX-treated *DD* plants than in ethanol solvent control (Fig 2C), indicating a reduced plastoquinol (PQ) reduction after MPK3/MPK6 activation. We next measured PQ redox status parameter 1-qL. Consistent with a decrease in PSII activity, a more oxidized PQ pool, reflected by the decrease of 1-qL, was detected (Fig 2D).

NPQ dissipates light energy as heat to protect PSII from photodamage [61,62]. We found that NPQ induction by high light (610 µmol m$^{−2}$ s$^{−1}$) was not affected at the early stage of MPK3/MPK6 activation but decreased significantly at 18 h and 24 h after DEX treatment (Fig 2E). The decreased NPQ at 18 h and 24 h is likely to be a consequence of PSII inhibition rather than an active down-regulation of NPQ. The decreased NPQ may accelerate PSII inhibition due to impaired dissipation of light energy.

We next examined PSII inhibition using blue native polyacrylamide gel electrophoresis (BN-PAGE), by which changes of thylakoid membrane photosynthetic complexes can be visualized. There was a decrease in PSII-LHCII super-complexes and an increase in CP43-less PSII
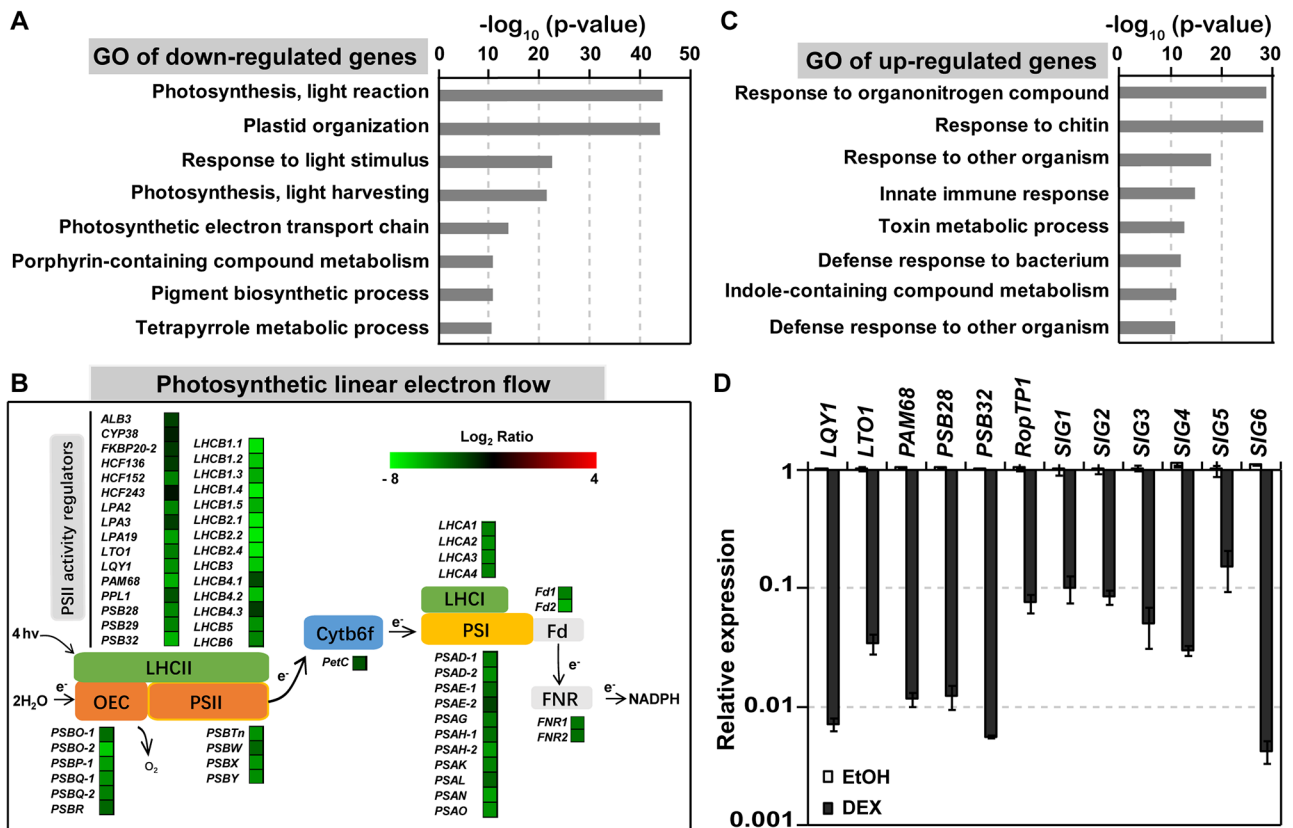
Fig 1. Activation of MPK3/MPK6 globally down-regulates photosynthetic genes. (**A**) GO enrichment of 2,977 down-regulated genes ($\log_2$ ratio $\leq$ −3) after MPK3/MPK6 activation. RNA-seq analysis was performed using 12-d-old *DD* seedlings treated with 5 μM DEX for 0 and 6 h under light. Transcript levels were fold changes relative to the 0 h sample. GO analysis was carried out by using DAVID online tool [57,58]. Enrichment scores are shown as $-\log_{10}$ (*p*-value). (**B**) Schematic diagram of photosynthetic linear electron flow. Expression levels of genes involved in photosystem assembly and repair are shown as a heat map. (**C**) GO enrichment of 1,039 up-regulated genes ($\log_2$ ratio $\leq$ −3) after MPK3/MPK6 activation. Enrichment scores are shown as $-\log_{10}$ (*p*-value). (**D**) Activation of MPK3/MPK6 induces drastic down-regulation of photosynthesis-related genes. Twelve-d-old *DD* plants grown in liquid medium were treated with EtOH or 5 μM DEX for 8 h under light. Transcript levels were quantified by real-time PCR and presented as fold changes relative to 0 h samples. Values are means ± SD, *n* = 3. *EF1a* was used as internal control, *n* = 3. The numerical values used to construct panels A–D can be found in S1 Data. See also S1 Table. Cytb6f, cytochrome b6f; DAVID, Database for Annotation, Visualization and Integrated Discovery; *DD*, GVG-NtMEK2^{DD}; DEX, dexamethasone; *EF1a*, elongation factor *1a*; EtOH, ethanol; Fd, ferredoxin; FNR, ferredoxin-NADP$^+$ reductase; GO, gene ontology; LHCI, light-harvesting complex I; LHCII, light-harvesting complex II; MPK, mitogen-activated protein kinase; OEC, oxygen-evolving complex; PSI, photosystem I; PSII, photosystem II; RNA-seq, RNA sequencing.

https://doi.org/10.1371/journal.pbio.2004122.g001

core complex in both BN-PAGE (Fig 2F) and two-dimensional sodium dodecyl sulfate (SDS)-PAGE analyses (S1 Fig), which correlates well with PSII inhibition. Collectively, the changes in photosynthetic parameters and complexes were found to be associated with the down-regulation in mRNA levels of photosynthetic genes after MPK3/MPK6 activation in *Arabidopsis* (Fig 1A). Together with our previous report that SIPK/WIPK activation inhibits photosynthetic activities in tobacco [32], we can conclude that inhibition of photosynthesis after the activation of pathogen-responsive MPK3/MPK6 in *Arabidopsis* or their orthologs in other plant species is a common response in plants.

Photosynthesis inhibition in plants frequently leads to the accumulation of ROS [63,64]. As shown in Fig 2G and S2 Fig, nitroblue tetrazolium (NBT) staining revealed an accumulation of superoxide ($O_2^{\bullet-}$) in the chloroplasts of *DD* plants after MPK3/MPK6 activation. This only occurred in plants kept under light. In the dark, no $O_2^{\bullet-}$ accumulation was observed. In chloroplasts, superoxide can be quickly converted to H_2O_2 under the action of superoxide dismutase.
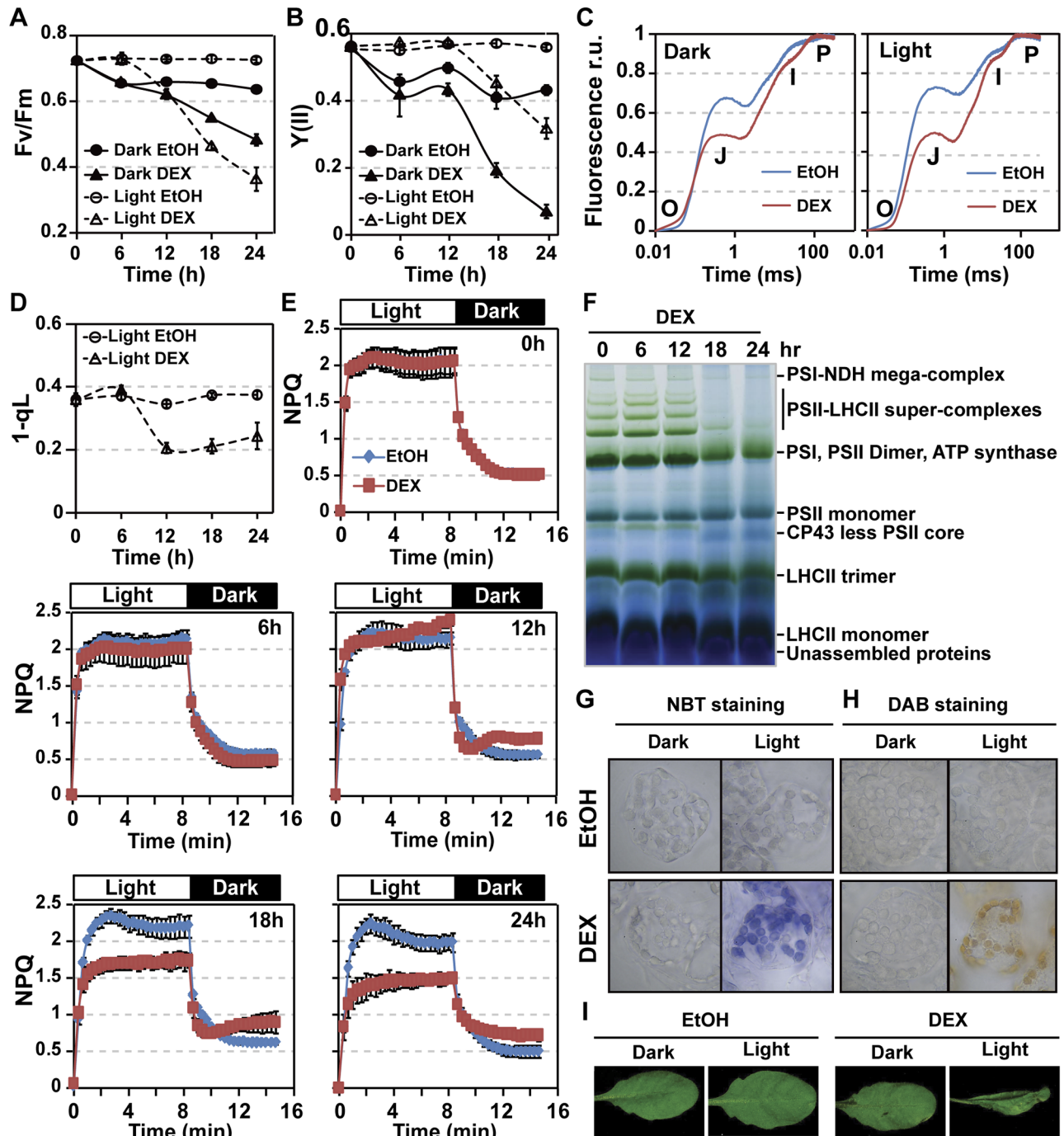
Fig 2. Activation of MPK3/MPK6 induces multilayered photosynthetic inhibition ROS accumulation in chloroplasts. (**A** and **B**) Activation of MPK3/MPK6 induces PSII inhibition. Fv/Fm (A) and Y(II) (B) were measured using soil-grown *DD* plants spray treated with EtOH (solvent control) or 15 μM DEX for indicated periods of time. Values are means ± SD, $n = 8$. (**C**) Changes of O-J-I-P curve induced by MPK3/MPK6 activation. Normalized fluorescence units were shown. Soil-grown *DD* plants were spray treated with EtOH or 15 μM DEX and kept in dark or light for 12 h. Representative measurements for each treatment were shown. (**D**) MPK3/MPK6 activation affects PQ pool redox status. Values are means ± SD, $n = 8$. (**E**) Activation of MPK3/MPK6 causes decreased NPQ at late stage. After treatment with EtOH or 15 μM DEX for indicated times under light, NPQ induction was carried out by using a light intensity of 610 μmol m^{-2} s^{-1} for 7 min and followed by an 8-min relaxation period in dark. Values are means ± SD, $n = 6$. (**F**) Activation of MPK3/MPK6 induces a decrease in PSII-LHCII super-complexes and an increase in CP43-less PSII core complex. Twelve-d-old *DD* plants grown in liquid medium were treated with 5 μM DEX for indicated times. Thylakoid membranes were isolated and solubilized with 1% dodecyl maltoside. Samples equivalent to 8 μg of chlorophyll were loaded to a BN-PAGE. (**G** and **H**) Activation of MPK3/MPK6 induces light-dependent accumulation of ROS in chloroplasts. *DD* plants grown in liquid medium were treated with EtOH solvent control or 5 μM DEX and kept in

dark or light for 8 h. Cellular $O_2^{\bullet-}$ (G) and H_2O_2 (H) were visualized by NBT and DAB staining, respectively. (**I**) Light accelerates MPK3/MPK6 activation-induced HR-like cell death. Soil-grown *DD* plants were first spray treated with EtOH solvent control or 15 μM DEX and then kept in dark or under light for 36 h. The numerical values used to construct panels A–E can be found in S1 Data. See also S1 and S2 Figs. BN-PAGE, blue native polyacrylamide gel electrophoresis; CP43, photosystem II chlorophyll protein of 43 kDa; DAB, 3,3′-diaminobenzidine; *DD*, *GVG-NtMEK2^{DD}*; DEX, dexamethasone; EtOH, ethanol; HR, hypersensitive response; LHCII, light-harvesting complex II; MPK, mitogen-activated protein kinase; NBT, nitroblue tetrazolium; NDH, NADH dehydrogenase-like; NPQ, non-photochemical quenching; PQ, plastoquinol; PSI, photosystem I; PSII, photosystem II; ROS, reactive oxygen species; r.u., relative unit.

Using 3,3′-diaminobenzidine (DAB) staining, we indeed detected the accumulation of H_2O_2 in chloroplasts after MPK3/MPK6 activation in a light-dependent manner (Fig 2H and S2 Fig). Consistent with our previous report using tobacco, MPK3/MPK6 activation-induced HR-like cell death in *Arabidopsis* was also light dependent (Fig 2I). It is worth noting that MPK3/MPK6 activation–induced PSII inhibition is independent of light, although it is delayed in the absence of light (Fig 2A and 2C), suggesting that ROS accumulation in chloroplasts may accelerate PSII inhibition and HR-like cell death in *DD* plants.

Long-lasting MPK3/MPK6 activation is needed to induce photosynthetic inhibition

Previous studies showed that MPK3/MPK6 activation is transient during PTI and is prolonged during CNL-type RPS2-mediated ETI [24]. To examine the amplitude of MPK3/MPK6 activation in regulating photosynthetic inhibition, *DD* plants were treated with increasing concentrations of DEX. As shown in Fig 3A, there was a correlation between the level of PSII inhibition and the amplitude of MPK3/MPK6 activation. Prolonged MPK3/MPK6 activation in *DD* caused a drastic photosynthetic inhibition, as demonstrated by western blot detection of PSII core proteins D1 (Fig 3B), while no photosynthetic inhibition was observed in Columbia-0 (Col-0) plants treated with a 22 amino acids flagellin fragment (flg22), which induced a transient MPK3/MPK6 activation (Fig 3B and S3 Fig). Moreover, MPK3/MPK6 activation-induced decrease of D1 protein is also independent of light (Fig 3C), which correlates well with the measured chlorophyll fluorescence in dark (Fig 2A–2C). To further test the duration of MAPK activation in regulating photosynthetic inhibition, we crossed *DD* transgene into *MPK6SR*, a chemical-genetically rescued *mpk3 mpk6* double mutant system [38,65], to generate *DD MPK6SR* (genotype: *GVG-NtMEK2^{DD} mpk3 mpk6 P_{MPK6}:MPK6^{YG}*). In *DD MPK6SR* plants, MPK6 can be activated by DEX and inhibited by 4-amino-1-tert-butyl-3-(1'-naphthyl) pyrazolo[3,4-d]pyrimidine (NA-PP1), a specific inhibitor of the sensitized *MPK6^{YG}*. As revealed by BN-PAGE analysis, short-term MPK6 activation failed to induce photosynthetic inhibition (Fig 3D), demonstrating that prolonged, but not transient, MAPK activation is required for photosynthetic inhibition. It was noted that photosynthetic inhibition in *DD MPK6SR* plants was slower in comparison to *DD* plants after DEX treatment, which may be due to the lack of *MPK3*, or reduced expression of NtMEK2^{DD} as a result of gene silencing, or both. Nonetheless, it clearly demonstrates that long-lasting, but not transient, MPK3/MPK6 activation induces photosynthetic inhibition.

ETI, but not PTI, induces prolonged MAPK activation, photosynthetic inhibition, and ROS accumulation in chloroplasts

To determine the involvement of MPK3/MPK6 in photosynthetic inhibition during plant immunity, we first measured the kinetics of photosynthetic parameters in wild-type plants infiltrated with *Pseudomonas syringae* pv. *tomato DC3000* carrying empty vector (*Pst-EV*), *Pst-AvrRpt2*, a *Pst* strain carrying the avirulence effector recognized by RPS2 (*AvrRpt2*) effector
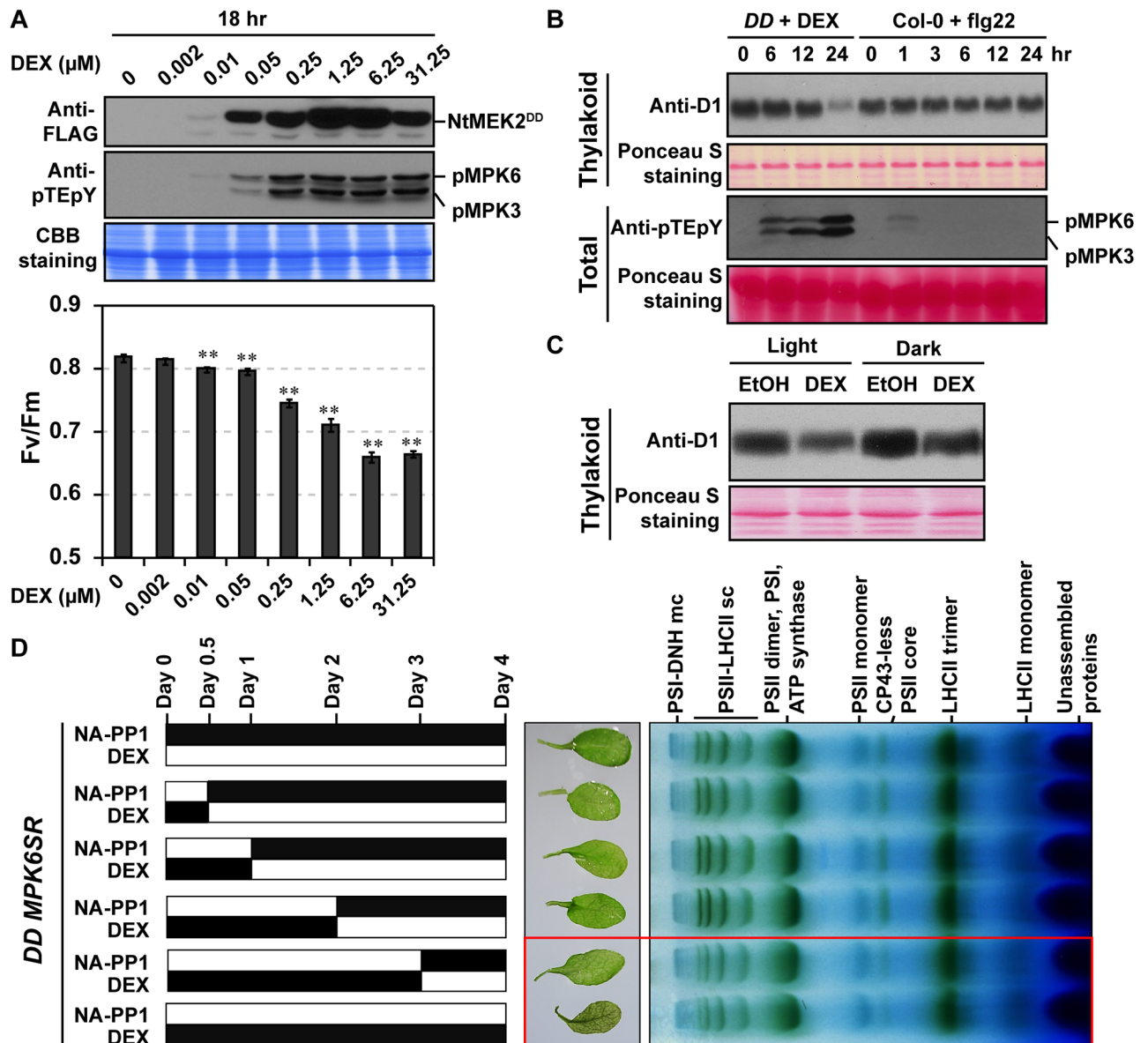
Fig 3. The amplitude and duration of MAPK activation regulate photosynthetic inhibition. (**A**) Controlling the amplitude of MPK3/MPK6 activation in *DD* plants by spraying different concentrations of DEX. Soil-grown *DD* plants were spray treated with different concentrations of DEX. At 9 h after DEX spray, NtMEK2^{DD} expression and MPK3/MPK6 activation were detected by immunoblot analysis using anti-FLAG and anti-pTEpY, respectively. Fv/Fm was measured at 18 h after DEX treatment. Values are means ± SD, $n = 6$, $^{**}P \leq 0.001$. The numerical values used to construct panel A can be found in S1 Data. (**B**) Transient activation of MPK3/MPK6 after flg22 treatment does not induce a decrease in PSII core D1 protein. Twelve-d-old *DD* and Col-0 plants grown in liquid medium were treated with 5 μM DEX and 200 nM flg22 for indicated times, respectively. Thylakoid membranes were isolated and solubilized with 1% dodecyl maltoside. Samples equivalent to 2 μg of chlorophyll were loaded to a 12% SDS-PAGE with 6 M urea. Anti-D1 was used to detect D1 abundance. MAPK activation was detected by immunoblot analysis using anti-pTEpY antibody. Ponceau S staining was used to show equal loading. (**C**) Twelve-d-old *DD* and Col-0 plants grown in ½ MS agar plates were treated with 5 μM DEX or EtOH (solvent control) and then kept in dark or under light for 12 h. D1 protein abundance in thylakoid membrane preparations was detected by immunoblot analysis using anti-D1 antibody. Ponceau S staining was used to show equal loading. (**D**) Prolonged, but not transient, MAPK activation induces photosynthetic inhibition. Twelve-d-old *DD MPK6SR* plants grown in liquid medium were first treated with 5 μM DEX. Seedlings were washed three times with ½ MS medium to remove DEX before the addition of 10 μM NA-PP1. Black bars indicate the durations of DEX or NA-PP1 treatment. Thylakoid membranes were isolated and solubilized with 1% dodecyl maltoside. Samples equivalent to 8 μg of chlorophyll were loaded to a BN-PAGE. See also S3 Fig. BN-PAGE, blue native polyacrylamide gel electrophoresis; CBB, Coomassie brilliant blue; Col-0, Columbia-0; CP43, photosystem II chlorophyll protein at 43 kDa; *DD*, *GVG-NtMEK2^{DD}*; DEX, dexamethasone; DNH, NADH dehydrogenase-like; EtOH, ethanol; FLAG, an octapeptide; flg22, a 22 amino acids flagellin fragment; LHCII, light-harvesting complex II; mc, mega-complex; MPK, mitogen-activated protein kinase; MS, Murashige and Skoog medium; NA-PP1, 4-amino-1-tert-butyl-3-(1'-naphthyl)pyrazolo[3,4-d]pyrimidine; pMPK, phosphorylated MPK; PSI, photosystem I; PSII, photosystem II; pTEpY, dually phosphorylated Thr/Glu/Tyr peptide; sc, super-complex; SDS-PAGE, sodium dodecyl sulfate-PAGE.

gene, or *Pst-hrcC⁻*, a *Pst* strain carrying a mutation in *hrcC* gene. *Pst-AvrRpt2* triggers both PTI and CNL-type *RPS2*-dependent ETI in *Arabidopsis*. Due to the lack of functional type-III secretion system, *Pst-hrcC⁻* cannot deliver effectors into plant cells and only induces PTI.

Similar to the gain-of-function activation of MPK3/MPK6 in *DD* plants, *Pst-AvrRpt2* induced drastic reductions in Fv/Fm (Fig 4A and S4 Fig), Y(II) (Fig 4B and S4 Fig), and 1-qL (Fig 4C). The decreases in Fv/Fm and Y(II) after *Pst-EV* inoculation were much slower and delayed in comparison to after *Pst-AvrRpt2* inoculation (Fig 4A and 4B and S4 Fig). Interestingly, *Pst-hrcC⁻*, which only induces PTI, had no effect on any measured chlorophyll fluorescence parameters (Fig 4A–4C and S4 Fig), indicating that PTI is not sufficient to induce photosynthetic inhibition. Consistent with this conclusion, flg22 infiltration failed to induce change in photosynthetic parameters and decrease of D1 protein (Fig 3B and S4 Fig). In addition, no photosynthetic changes were detected after infiltration of a nonpathogenic strain, *P. fluorescens*, carrying empty vector [66], while *P. fluorescens* carrying *AvrRpm1*, which triggers CNL-type RPM1-mediated ETI, induced strong photosynthetic inhibition (S4 Fig). These results further support that ETI, but not PTI, induces photosynthetic inhibition.

The interaction between *Pst-AvrRpt2* and *Arabidopsis* is complex, involving both virulent and avirulent effectors that can induce effector-triggered susceptibility (ETS) and ETI, respectively, besides PTI. To determine whether ETI is sufficient to induce PSII inhibition, we utilized the DEX-inducible promoter-driven *AvrRpt2* (*GVG-AvrRpt2*) transgenic plants [67]. DEX treatment of *GVG-AvrRpt2* plants is sufficient to activate MPK3/MPK6 in a *RPS2*-dependent manner [25]. Similar to MPK3/MPK6 activation and *Pst-AvrRpt2* inoculation, DEX treatment of *GVG-AvrRpt2* plants was sufficient to induce drastic PSII inhibition (Fig 4D and 4E) and PQ pool oxidation (Fig 4F). Similarly (Fig 2G and 2H), induction of *AvrRpt2* expression also led to the accumulation of $O_2^{\bullet-}$ and H_2O_2 in chloroplasts (S5 Fig). In *rps2* mutant background, AvrRpt2-induced photosynthetic inhibition and accumulation of ROS in chloroplasts were abolished (Fig 4D–4F and S5 Fig), demonstrating that AvrRpt2 effector is sufficient to induce photosynthetic inhibition and ROS generation in an RPS2-dependent fashion.

We also tested MAPK activation and chlorophyll fluorescence parameters after infiltrating with *Pst-AvrRpm1*, *Pst-AvrB* and *Pst-AvrRps4*. Among the four tested effectors, AvrRpt2 and AvrRpm1 induce CNL NLR-dependent ETI [68–72], AvrB induces both CNL and TNL NLR-dependent ETI [70,72,73], and AvrRps4 induces TNL NLR-dependent ETI [74,75]. Interestingly, we found TNL ETI also induces prolonged MAPK activation and PSII inhibition (Fig 4G and S6 Fig), indicating that MAPK signaling and its activation-mediated photosynthetic inhibition and chloroplastic ROS accumulation are essential for both CNL and TNL NLR-conditioned ETI.

MPK3 and MPK6 are required for both CNL- and TNL-mediated ETI

To determine whether MPK3/MPK6 are required for ETI-induced photosynthetic inhibition and ROS accumulation in chloroplasts, we utilized the newly generated chemical-genetically rescued *mpk3 mpk6* double mutant systems [38,65]. Both *MPK6SR* (genotype: *mpk3 mpk6 P_{MPK6}:MPK6^{YG}*) and *MPK3SR* (genotype: *mpk3 mpk6 P_{MPK3}:MPK3^{TG}*) were tested. As is shown in Fig 5A, *Pst-AvrRpt2*–induced PSII inhibition was partially impaired in *MPK6SR* and *MPK3SR* plants after pretreatment with NA-PP1, a specific inhibitor of the sensitized *MPK6^{YG}* and *MPK3^{TG}*, demonstrating that MPK3 and MPK6 are required for the fast and drastic PSII inhibition triggered by ETI activation. No differences were observed in *MPK6SR* and *MPK3SR* plants pretreated with DMSO (Fig 5B), or *mpk3* and *mpk6* single mutants (Fig 5C), demonstrating that MPK3 and MPK6 function redundantly in mediating ETI-induced PSII inhibition.
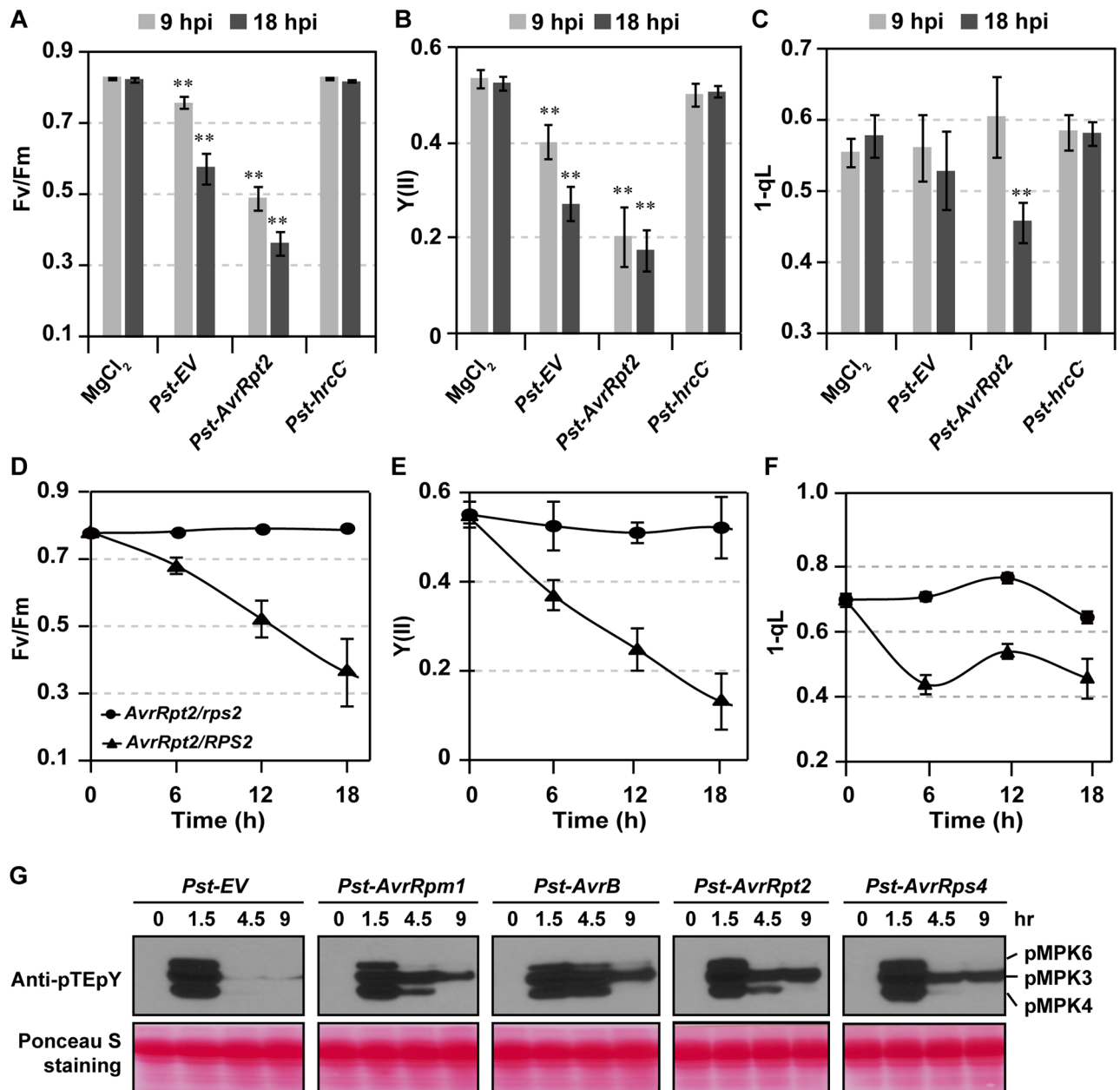
Fig 4. ETI induces strong PSII inhibition and prolonged MAPK activation. (**A–C**) Photosynthetic parameters are differentially affected by different *Pst* strains. Four-wk-old Col-0 plants were infiltrated with 10 mM $MgCl_2$ (mock), *Pst-EV*, *Pst-AvrRpt2*, or *Pst-hrcC*⁻ (OD_{600} = 0.2) and then were kept under light with a transparent lid. Photosynthetic parameters, including Fv/Fm (A), Y(II) (B), and 1-qL (C), were measured at 9 and 18 hpi. Values are means ± SD, n = 5–8, $**P \leq 0.001$. (**D–F**) AvrRpt2-triggered immunity induces drastic PSII inhibition. Four-wk-old soil-grown *GVG-AvrRpt2* transgenic plants in Col-0 (*AvrRpt2/RPS2*) or *rps2* mutant background (*AvrRpt2/rps2*) were spray treated with 15 μM DEX. Photosynthetic parameters, including Fv/Fm (D), Y(II) (E), and 1-qL (F), were measured at indicated times. Values are means ± SD, n = 4–8. The numerical values used to construct panels A–F can be found in S1 Data. (**G**) ETI mediated by both CNL- and TNL-type NLRs induces prolonged MAPK activation. Four-wk-old Col-0 plants were infiltrated with *Pst* carrying *EV*, *AvrRpm1*, *AvrB*, AvrRpt2, or *AvrRps4* (OD_{600} = 0.02) for indicated time points. MPK3/MPK6 activation was detected by anti-pTEpY antibody. See also S4 and S5 Figs. *AvrB*, avirulence protein B; *AvrRpm1*, avirulence effector recognized by RPM1; *AvrRpt2*, avirulence effector recognized by RPS2; *AvrRps4*, avirulence effector recognized by RPS4; CNL, coiled coil-nucleotide binding site-leucine rich repeat; Col-0, Columbia-0; DEX, dexamethasone; ETI, effector-triggered immunity; EV, empty vector; *GVG-AvrRpt2*, DEX-inducible promoter-driven *AvrRpt2*; hpi, hours post inoculation; *hrcC*⁻, outer membrane type III secretion protein HrcC mutant; MPK, mitogen-activated protein kinase; NLR, nucleotide-binding leucine-rich repeat; OD, optical density; pMPK, phosphorylated MPK; PSII, photosystem II; *Pst*, *Pseudomonas syringae* pv *tomato*; pTEpY, dually phosphorylated Thr/Glu/Tyr peptide; RPS2, Resistance to *Pseudomonas syringae* 2; TNL, Toll/interleukin-1 receptor-nucleotide binding site-leucine rich repeat.
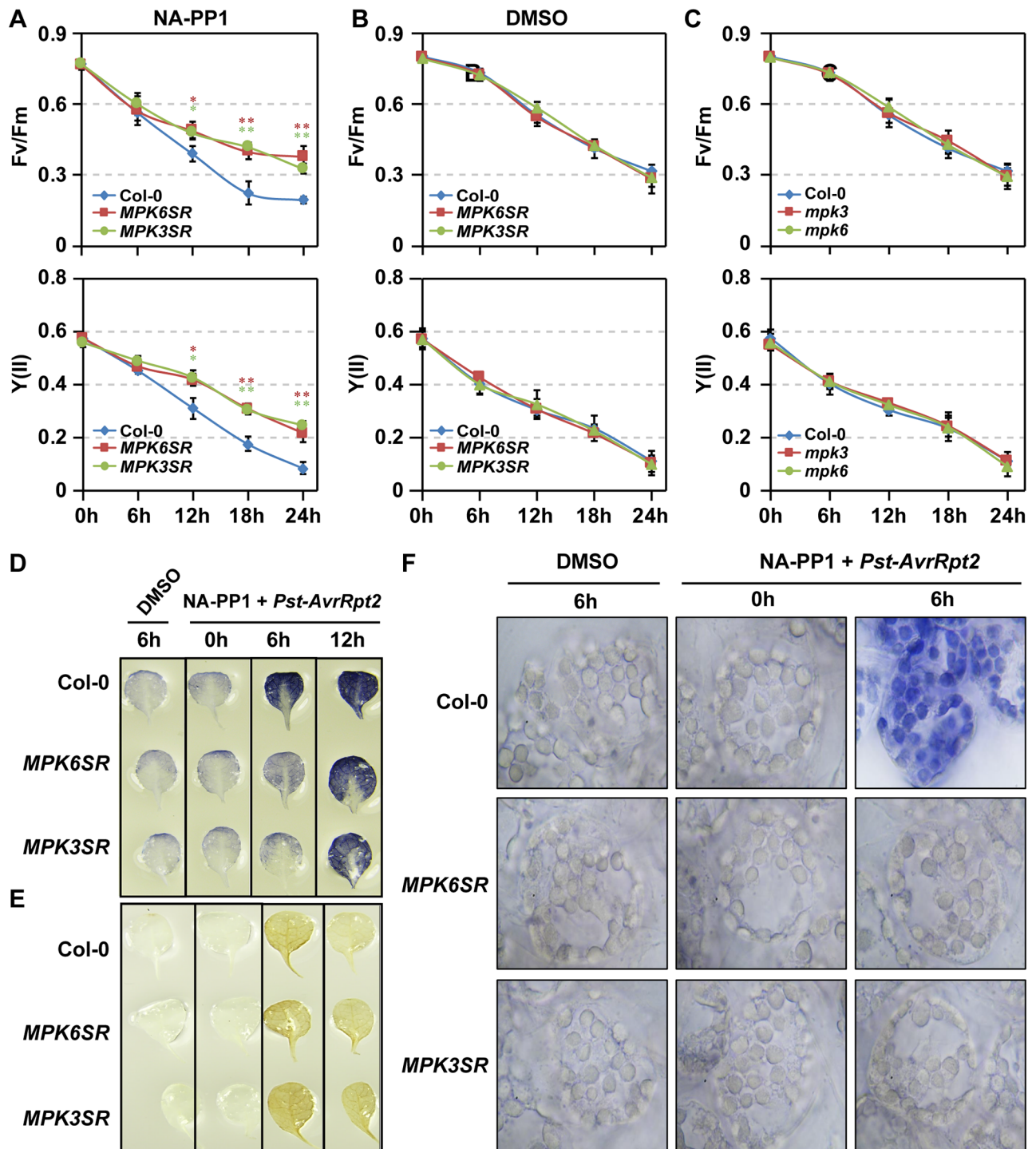
https://doi.org/10.1371/journal.pbio.2004122.g004

Fig 5. MPK3 and MPK6 are required for ETI-induced PSII inhibition and ROS accumulation in chloroplasts. (A and B) *Pst-AvrRpt2*–induced PSII inactivation is partially compromised in *mpk3 mpk6* double mutant. Four-wk-old soil-grown Col-0, *MPK6SR*, and *MPK3SR* plants were first spray treated with NA-PP1 (10 μM) or DMSO solvent control for 2 h and then infiltrated with *Pst-AvrRpt2* (OD = 0.2). Values are means ± SD, $n = 4$, $0.01 \leq$ $^{*}P \leq 0.001$ and $^{**}P \leq 0.001$. (C) Normal *Pst-AvrRpt2*–induced PSII inactivation in *mpk3* and *mpk6* single mutants. Four-wk-old soil-grown Col-0, *mpk3*, and *mpk6* plants were directly infiltrated with *Pst-AvrRpt2* (OD = 0.2). Fv/Fm and Y(II) were measured at indicated time points. Values are means ± SD, $n = 4$. The numerical values used to construct panels A–C can be found in S1 Data. (D–F) MPK3 and MPK6 are required for *Pst-AvrRpt2*–induced $O_2^{\bullet-}$, but not H_2O_2, accumulation. Twelve-d-old Col-0, *MPK6SR*, and *MPK3SR* plants grown in liquid medium were first treated with 2 μM NA-PP1 or DMSO (mock) for 1 h. They were then treated with *Pst-AvrRpt2* (OD$_{600}$ = 0.02) for indicated periods of time. $O_2^{\bullet-}$ and H_2O_2 accumulation were detected by NBT and DAB staining, respectively. *AvrRpt2*, avirulence effector recognized by RPS2; Col-0, Columbia-0; DAB, 3,3′-

diaminobenzidine; ETI, effector-triggered immunity; MPK, mitogen-activated protein kinase; NA-PP1, 4-amino-1-tert-butyl-3-(1'-naphthyl)pyrazolo [3,4-d]pyrimidine; NBT, nitroblue tetrazolium; OD, optical density; $O_2^{\bullet-}$, superoxide; *Pst*, *Pseudomonas syringae* pv *tomato*; PSII, photosystem II; ROS, reactive oxygen species.

We next examined *MPK6SR* and *MPK3SR* plants inoculated with *Pst-AvrRpt2* to determine whether MPK3 and MPK6 are required for the ETI-mediated increase in $O_2^{\bullet-}/H_2O_2$. As shown in Fig 5D and 5F, *Pst-AvrRpt2*–induced $O_2^{\bullet-}$ accumulation in chloroplasts was delayed in NA-PP1–treated *MPK6SR* and *MPK3SR*, which correlates well with the reduced PSII inhibition in NA-PP1–treated *MPK6SR* and *MPK3SR* plants (Fig 5A). These results suggest that MPK3/MPK6 are involved in ETI-induced ROS accumulation in chloroplasts. However, although MPK3/MPK6 activation can induce both accumulation of H_2O_2 and $O_2^{\bullet-}$ (Fig 2G and 2H and S2 Fig), *Pst-AvrRpt2*–induced H_2O_2 accumulation was not affected in *MPK6SR* and *MPK3SR* (Fig 5E), possibly due to the complicated enzymatic and nonenzymatic conversion of $O_2^{\bullet-}$ to H_2O_2 and/or H_2O_2 decomposition.

Although HR-like cell death after the activation of MPK3/MPK6 or their orthologs in tobacco was detailed more than a decade ago [52,76,77], it is still unknown whether pathogen-induced HR cell death requires this MAPK cascade. As a result, we examined HR cell death in *MPK3SR* and *MPK6SR* during ETI after *Pst-AvrRpt2* inoculation. As shown in Fig 6A and 6B, HR cell death and ion leakage were impaired in NA-PP1–, but not DMSO–, treated *MPK6SR* and *MPK3SR* plants. Associated with this, we also observed compromised resistance to *Pst-AvrRpt2* in NA-PP1–treated *MPK6SR* and *MPK3SR* plants (Fig 6C). Associated with the high titer of *Pst-AvrRpt2* growth in *Arabidopsis*, leaf chlorosis was observed (Fig 6C), consistent with the breach of plant ETI in the loss-of-function *mpk3 mpk6* double mutant system. In solvent DMSO-treated controls, the growth of *Pst-AvrRpt2* was suppressed, demonstrating an effective ETI (Fig 6C). These results demonstrate that MPK3 and MPK6 function redundantly and are required for ETI.

We also measured PSII inhibition, ion leakage, and bacterial growth in the loss-of-function *mpk3 mpk6* double mutant system after inoculation with *Pst* carrying *AvrRpm1*, *AvrB*, and *AvrRps4*. As shown in S6 Fig, PSII inhibition and ETI were all compromised in NA-PP1–, but not DMSO–, treated *MPK6SR* and *MPK3SR* plants. These results suggest that MPK3/MPK6 are essential for both CNL- and TNL-type NLR-mediated PSII inhibition and ETI.

Prolonged, but not transient, MAPK activation induces photosynthetic inhibition (Fig 3B). As a result, we examined whether long-lasting MAPK activation is essential for ETI. Wild-type *MPK6SR* and *MPK3SR* plants infiltrated with *Pst-AvrRpt2* were treated with NA-PP1 to inhibit MAPK activity at different times after inoculation. As shown in Fig 6D, NA-PP1 treatment at 12 hpi could still compromise RPS2-mediated ETI, demonstrating that short-term MAPK activation was not sufficient to confer efficient ETI.

Photosynthetic inhibition is essential to ETI

To provide genetic evidence to support the importance of photosynthetic inhibition in ETI, we expressed a plastid-targeted cyanobacterial flavodoxin (pFld) in *DD* and *GVG-AvrRpt2* plants. Flowering plants do not have flavodoxin [78], and ectopically expressing a cyanobacterial flavodoxin in tobacco confers broad stress tolerance [79,80]. We found that overexpression of pFld in *DD* and *GVG-AvrRpt2* background caused growth retardation (Fig 7A and 7B, and S7 Fig). This is likely a result of the lower efficiency of flavodoxin as an electron carrier in comparison to ferredoxin [78,81]. Nonetheless, we observed that PSII inhibition induced by MPK3/MPK6 activation was impaired in pFld-overexpressing plants. Two independent pFld expression lines were used. Neither line, the induction of DD protein nor the activation of
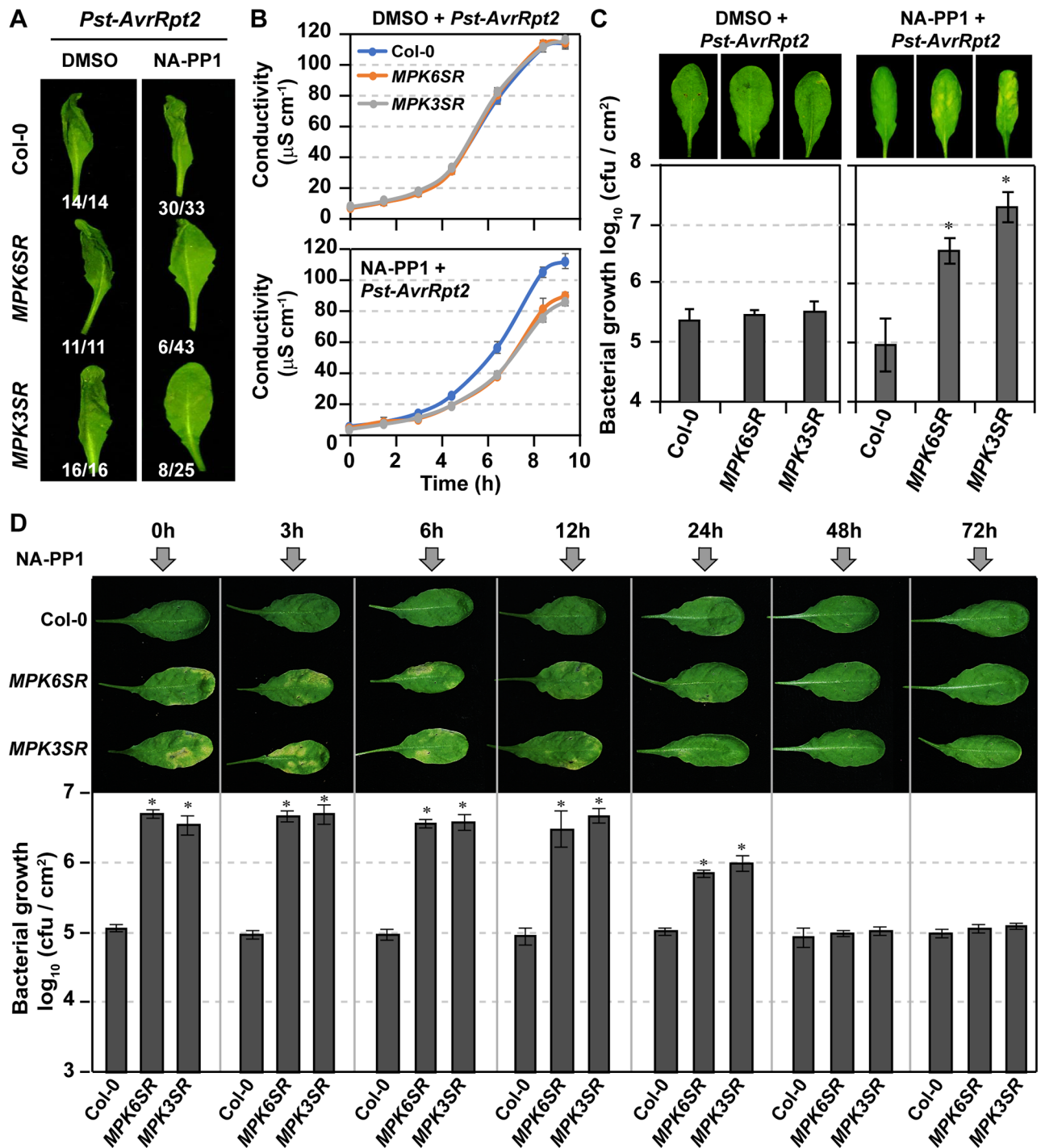
Fig 6. Prolonged MPK3/MPK6 activation is essential to ETI. (**A**) MPK3 and MPK6 are required for *Pst-AvrRpt2*–induced HR cell death. Soil-grown Col-0, *MPK6SR*, and *MPK3SR* plants were first spray treated with 10 μM NA-PP1 for 2 h and then infiltrated with *Pst-AvrRpt2* (OD = 0.02). Photos were taken at 18 hpi. Numbers are ratios of leaves with HR phenotype. (**B**) MPK3 and MPK6 are required for *Pst-AvrRpt2*–induced ion leakage. Soil-grown Col-0, *MPK6SR*, and *MPK3SR* plants were first spray treated with 10 μM NA-PP1 for 2 h; leaf discs were punched and then infiltrated with *Pst-AvrRpt2* (OD = 0.02) by vacuum. Leaf discs were then transferred to GC vials containing 2 μM NA-PP1 or DMSO. Ion leakage was measured as increase in conductivity. Values are means ± SD, n = 4. (**C**) MPK3 and MPK6 are required for disease resistance against *Pst-AvrRpt2*. Col-0, *MPK6SR*, and *MPK3SR* plants grown in soil were first spray treated with 10 μM NA-PP1 or DMSO and then infiltrated with *Pst-AvrRpt2* (OD$_{600}$ = 0.0005). NA-PP1 or DMSO was sprayed again at 1.5 dpi. *Pst-AvrRpt2* growth was quantified at 3 dpi. Values are means ± SD, n = 3, $0.01 \leq {}^*P \leq 0.001$. (**D**) Prolonged activation of MPK3/MPK6 is required for ETI-mediated resistance. Col-0, *MPK6SR*, and *MPK3SR* plants grown in soil were infiltrated with *Pst-AvrRpt2* (OD$_{600}$ = 0.0005). NA-PP1 was sprayed at indicated time points. *Pst-AvrRpt2* growth was quantified at 3 dpi. Values are means ± SD, n = 3,

MPK3/MPK6 after DEX treatment, was affected by the overexpression of pFld (Fig 7C). As shown in Fig 7D, expression of pFld impaired MPK3/MPK6 activation-mediated ROS accumulation. Concomitantly, PSII inhibition, disassembly of photosynthetic complexes and HR-like cell death were all delayed (Fig 7E–7G). Expression of pFld also alleviated the photosynthetic inhibition triggered by conditional expression of *AvrRpt2* (S7 Fig).

To test whether the inhibition of photosynthetic activities in chloroplasts is required for the robustness of ETI, we infiltrated *DD*, *DD/pFld-7*, and *DD/pFld-8* with *Pst-AvrRpt2*. In the absence of DEX, *DD* transgene is not expressed, and these plants can be treated as wild-type control and *pFld* transgenic plants, respectively. PSII inhibition induced by *Pst-AvrRpt2* was greatly delayed in *DD/pFld-7* and *DD/pFld-8* plants, which was associated with the inhibition of HR cell death (Fig 8A), a compromised resistance (Fig 8B), impaired ROS accumulation (Fig 8C), and delayed disassembly of photosynthetic complexes (S8 Fig). The elevated *Pst-AvrRpt2* growth led to chlorosis, a susceptible phenotype (Fig 8B). These results strongly suggest that inhibition of photosynthetic activity is essential to ETI. This notion is further supported by the observation that HR cell death and PSII inactivation is delayed in dark (Fig 7D), in which no ROS accumulation in chloroplasts was observed (Fig 2G and 2H and S5 Fig). In addition, disease resistance to *Pst-AvrRpt2* was also greatly compromised in dark or under low light, and *Pst-AvrRpt2* grew to higher titers and caused chlorosis, symptoms of susceptibility (Fig 8E and 8F). Altogether, these results suggest that light-dependent ROS accumulation in chloroplasts is an important part of ETI.

Discussion

Decrease in plant photosynthetic activity and global down-regulation of photosynthetic genes have long been associated with plants under biotic stresses [44–50]. However, it is unclear whether this is a reflection of deterioration of plant health or an active part of plant immunity. Recently, we reported the essential role of MPK3/MPK6 in plant PTI [38]. MPK3 and MPK6 are also activated during ETI [24,25]. However, genetic evidence demonstrating the requirement of MPK3/MPK6 in ETI is still lacking. In this report, we demonstrate that gain-of-function activation of MPK3/MPK6 in *Arabidopsis* is sufficient to induce active inhibition of photosynthesis and light-dependent ROS accumulation in chloroplasts, two processes that mutually enhance each other under light. Loss-of-function data revealed that MPK3 and MPK6 are essential to effector-triggered photosynthetic inhibition and ROS accumulation in chloroplasts, and eventually ETI. This study highlights the important role of MPK3/MPK6-mediated photosynthetic inhibition and ROS accumulation in chloroplasts during ETI, which can explain why plants are more resistant under light than in dark. We propose that active photosynthetic inhibition mediated by the MPK3/MPK6 pathway is one of the key immune responses downstream of NLR activation and contributes to a robust ETI (Fig 8G).

MPK3/MPK6 activation induces light-independent photosynthetic inhibition and light-dependent ROS accumulation in chloroplasts

MPK3/MPK6 activation-induced HR-like cell death and ROS accumulation in chloroplasts are light dependent (Fig 2G–2I). This is also true in a tobacco system [32]. However, MPK3/MPK6 activation-induced PSII inhibition can be independent of light (Figs 2A–2C and 3C).
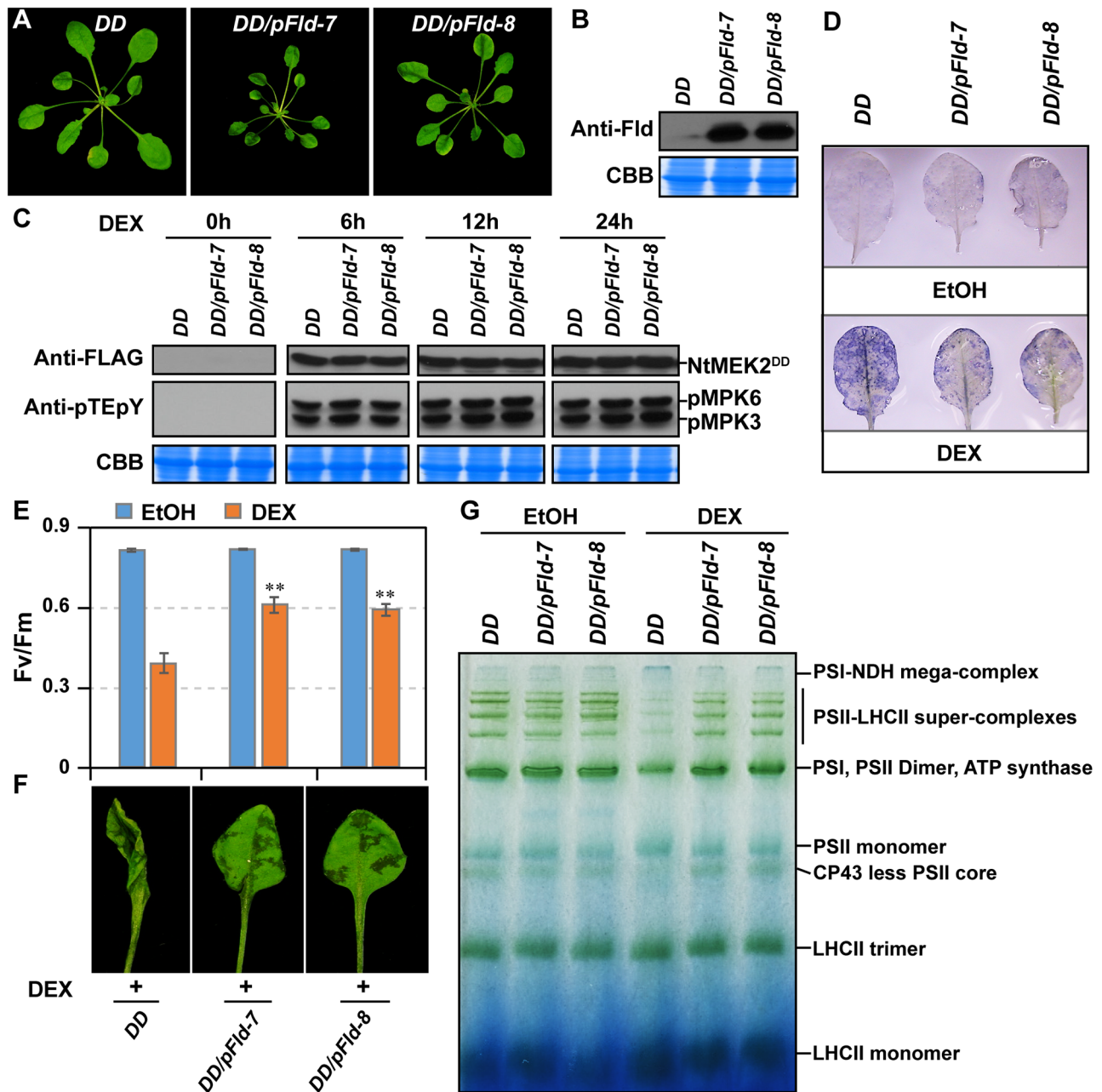
Fig 7. Expression of pFld impairs MPK3/MPK6 activation-induced ROS accumulation, PSII inhibition, and HR-like cell death. (A) Phenotype of 4-wk-old *pFld* transgenic plants in *DD* background. (B) Immunoblot analysis of pFld expression using anti-Fld antibody. (C) Normal activation of MPK3/MPK6 in *pFld* transgenic plants. Soil-grown plants were spray treated with 15 μM DEX for indicated periods of time. *DD* expression and activation of MPK3/MPK6 activation were detected by using anti-FLAG and anti-pTEpY, respectively. (D) Overexpression of *pFld* suppresses MPK3/MPK6 activation-induced ROS accumulation. Soil-grown *DD* and *DD/pFld* plants were infiltrated with EtOH or 5 μM DEX. $O_2^{\bullet-}$ was visualized by NBT staining. (E–G) Overexpression of *pFld* suppresses MPK3/MPK6 activation-induced photosynthetic inhibition. Fv/Fm was measured at 24 h (E), HR-like phenotype was recorded at 30 h (F), and disassembly of photosynthetic complexes at 24 h was visualized by BN-PAGE (G). Samples equivalent to 8 μg of chlorophyll were loaded. Values are means ± SD, $n = 6$, [**]$P \leq 0.001$. The numerical values used to construct panel E can be found in S1 Data. See also S7 Fig. BN-PAGE, blue native polyacrylamide gel electrophoresis; CBB, Coomassie brilliant blue; CP43, photosystem II chlorophyll protein of 43 kDa; *DD*, *GVG-NtMEK2^DD*; DEX, dexamethasone; EtOH, ethanol; FLAG, an octapeptide; Fld, flavodoxin; HR, hypersensitive response; LHCII, light-harvesting complex II; MPK, mitogen-activated protein kinase; NtMEK2^DD, constitutively activated NtMEK2; NBT, nitroblue tetrazolium; NDH, NADH dehydrogenase-like; $O_2^{\bullet-}$, superoxide; *pFld*, plastid-targeted cyanobacterial flavodoxin; pMPK, phosphorylated MPK; PSI, photosystem I; PSII, photosystem II; pTEpY, dually phosphorylated Thr/Glu/Tyr peptide; ROS, reactive oxygen species.
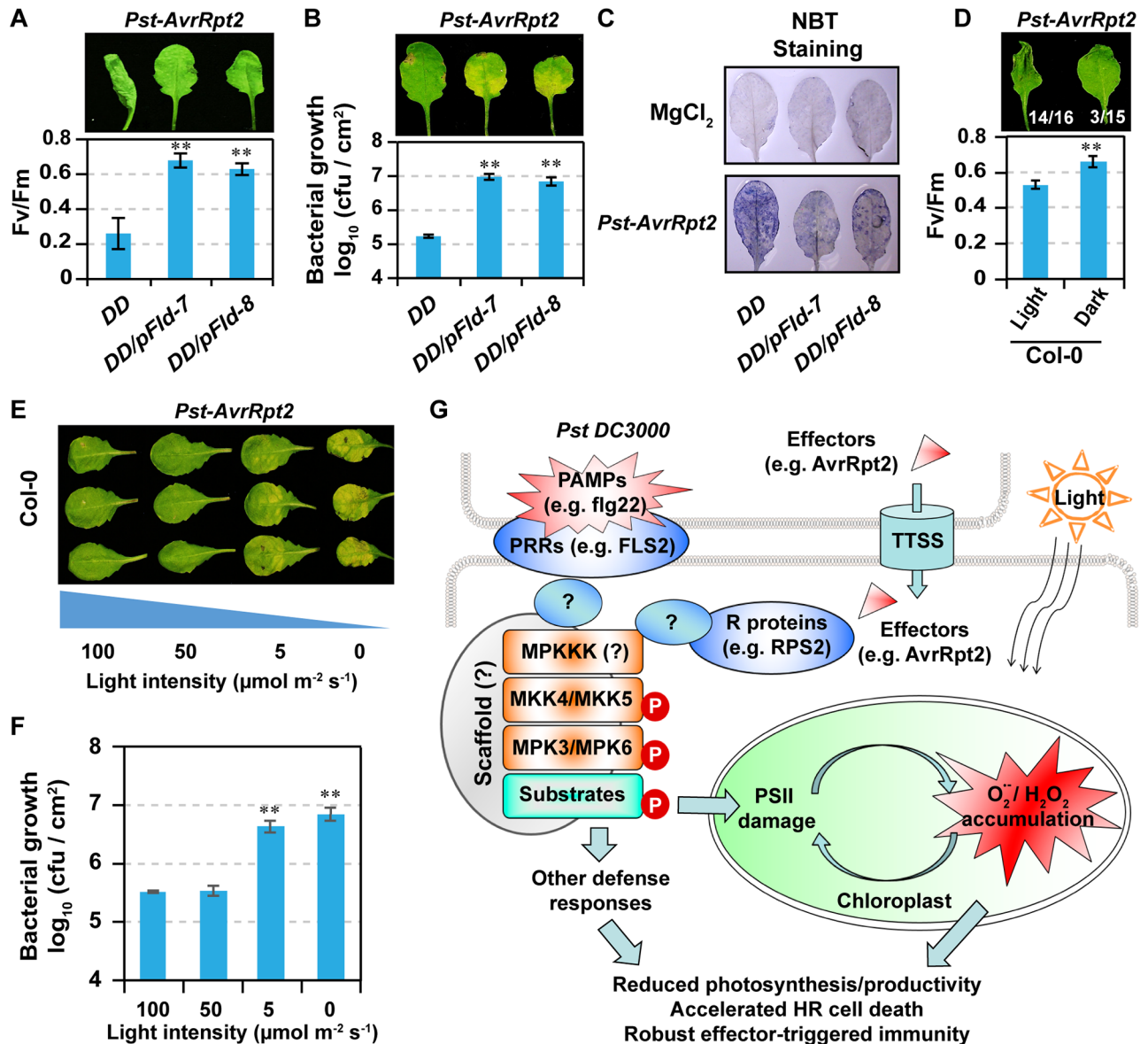
https://doi.org/10.1371/journal.pbio.2004122.g007

Fig 8. Photosynthetic inhibition and light are essential to a robust ETI. (**A**) Expression of *pFld* suppresses *Pst-AvrRpt2*–induced HR phenotype and PSII inhibition. Soil-grown *DD* and *DD/pFld* plants were infiltrated with *Pst-AvrRpt2* (OD = 0.02). Photos were taken at 24 hpi. Fv/Fm was measured at 18 hpi. Values are means ± SD, $n = 6$, $**P \leq 0.001$. (**B**) Expression of *pFld* compromises disease resistance against *Pst-AvrRpt2*. Four-wk-old soil-grown *DD* and *DD/pFld* plants were infiltrated with *Pst-AvrRpt2* ($OD_{600} = 0.0005$). Photos were taken at 3 dpi and *Pst-AvrRpt2* growth was quantified at 2.5 dpi. Values are means ± SD, $n = 3$, $**P \leq 0.001$. (**C**) Expression of *pFld* impairs *Pst-AvrRpt2*–induced ROS accumulation. Soil-grown *DD* and *DD pFld* plants were infiltrated with mock (10 mM $MgCl_2$) or *Pst-AvrRpt2* (OD = 0.02). $O_2^{\bullet-}$ was visualized by NBT staining at 6 hpi. (**D**) Light accelerates *Pst-AvrRpt2*–induced PSII inhibition and HR cell death. Four-wk-old Col-0 plants were infiltrated with *Pst-AvrRpt2* (OD = 0.02). Plants were kept in dark or under light. Photos were taken at 18 hpi and numbers are ratios of leaves with HR phenotype. Fv/Fm was measured at 12 hpi. Values are means ± SD, $n = 7$, $**P \leq 0.001$. (**E** and **F**) Light is essential to plant resistance against *Pst-AvrRpt2*. Four-wk-old Col-0 plants were infiltrated with *Pst-AvrRpt2* (OD = 0.0005). After infiltration, plants were kept under light for 2 h to allow the evaporation of liquid, and then kept in dark or under different light intensities, as indicated. Photos were taken and *Pst-AvrRpt2* growth was determined at 3 dpi. Values are means ± SD, $n = 3$, $**P \leq 0.001$. The numerical values used to construct panels A, B, D, and F can be found in S1 Data. (**G**) Schematic model of MPK3/MPK6 activation-induced PSII inhibition, ROS accumulation in chloroplasts, and the robustness of ETI. *AvrRpt2*, avirulence effector recognized by RPS2; Col-0, Columbia-0; *DD*, *GVG-NtMEK2^DD*; dpi, days post inoculation; ETI, effector-triggered immunity; flg22, a 22 amino acids flagellin fragment; FLS2, flagellin-sensitive 2; hpi, hours post inoculation; HR, hypersensitive response; MPK, mitogen-activated protein kinase; NBT, nitroblue tetrazolium; OD, optical density; $O_2^{\bullet-}$, superoxide; PAMP, pathogen/microbe-associated molecular pattern; *pFld*, plastid-targeted cyanobacterial flavodoxin; PRR, pattern recognition receptor; *Pst*, *Pseudomonas syringae* pv *tomato*; PSII, photosystem II; ROS, reactive oxygen species; RPS2, Resistance to *Pseudomonas syringae* 2; TTSS, type III secretion system.

We also noticed that PSII inhibition was slower in the absence of light, which could be a result of the lack of ROS generation (Fig 2G and 2H). ROS are known to play an important role in accelerating PSII inhibition by oxidative damage of PSII proteins [82–84]. Under light, MPK3/MPK6 activation-induced PSII inactivation and ROS accumulation in chloroplasts can form a positive feed-forward loop to accelerate the PSII inhibition. Nonetheless, MPK3/MPK6 activation-induced photosynthetic inhibition can occur in the absence of light and be independent of chloroplastic ROS accumulation.

MPK3/MPK6-mediated inhibition of photosynthesis is an important part of both CNL- and TNL-type NLR-mediated ETI

Photosynthetic inhibition is a well-documented phenomenon in plants challenged by pathogens [46–50,85–88]. However, it was not clear whether photosynthetic inhibition is a programmed part of immune response or merely a side effect caused by pathogen infection. In this study, we provided several lines of evidence suggesting that photosynthetic inhibition is an active defense response and an important part of ETI. First of all, AvrRpt2-induced photosynthetic inhibition requires its immune receptor, RPS2, demonstrating that photosynthetic inhibition is an event downstream of NLR activation. Secondly, prolonged activation of MPK3/MPK6, an event downstream of NLR activation in ETI [24], induces photosynthetic inhibition. Thirdly, ETI and MAPK signaling–mediated photosynthetic inhibition facilitate ROS accumulation in chloroplasts, which is essential to ETI. Previous studies demonstrate that light is essential for virus-induced HR [32,89]. In this study, we also found an essential role of light in *Pst-AvrRpt2*–induced HR and plant resistance against *Pst-AvrRpt2* (Fig 8D–8F). Thus, photosynthetic inhibition during ETI is actively regulated and is part of the immune response that enhances resistance.

We found that *Pst-AvrRps4* also induces prolonged MAPK activation (Fig 4G), although AvrRps4 is sensed by RPS4/RRS1, a TNL-type NLR, which was thought to function in nuclei mainly through transcriptional reprogramming [12]. The requirement of MPK3/MPK6 in both CNL- and TNL-mediated ETI raises a question of how NLR activation leads to prolonged MPK3/MPK6 activation. MPK4 is guarded by CNL-type R protein, suppressor of *mkk1 mkk2* (SUMM2), which monitors the phosphorylation status of MPK4 substrates, including MAP kinase kinase kinase 2 (MEKK2), mRNA de-capping protein PAT1, and calmodulin binding receptor-like cytoplasmic kinase 3 (CRCK3) [90–93]. It remains to be determined whether MPK3 and MPK6 are also protected by CNL- or TNL-type R proteins. In PTI, MPK3/MPK6 activation after PAMP perception by PRRs can be mediated by receptor-like cytoplasmic kinases (RLCKs), which are similar to RLKs but lack an extracellular domain. *Arabidopsis* RLCK PBS1-like 27 (PBL27) and rice (*Oryza sativa*) OsRLCK85 were demonstrated to connect chitin perception to MPK3/MPK6 activation [94,95]. It will be interesting to identify the proteins that connect NLRs to MPK3/MPK6, which may reveal the mechanism(s) underlying the prolonged activation of MPK3/MPK6 during ETI.

MPK3/MPK6 cascade regulates the trade-off between growth and defense in plant immunity

The concept of a trade-off between growth and defense has been proposed for many decades [96]. Our current knowledge on the growth–defense trade-off mainly stems from antagonistic cross talk among hormones that promote defense and that promote growth, such as SA-auxin, SA-brassinosteroid (BR), SA-gibberellic acid (GA), jasmonic acid (JA)-Auxin, JA-BR, and JA-GA [97–99]. However, how a plant integrates multiple internal and external stimuli to shift the balance between growth and defense remains poorly understood. It is also unclear why

these two events are coupled together most of the time. We showed in this report that both events are regulated by the same MAPK signaling pathway. MPK3/MPK6 activation globally down-regulates photosynthetic genes and, in the meantime, up-regulates numerous defense-related genes (Fig 1A–1C), suggesting that MAPK signaling plays important roles in orchestrating growth and defense in plant immunity. Consistent with the down-regulation of photosynthetic genes, we did observe decreases in CO_2 fixation [32] and photosynthetic inhibition (Fig 2A–2C). Both would have negative impacts on normal plant growth and development. In the meantime, up-regulation of defense genes by the MPK3/MPK6 cascade leads to an increased biosynthesis of defense-related secondary metabolites such as camalexin [53] and indole glucosinolate derivatives [56]. Considering that multiple developmental and environmental signals converge at the MPK3/MPK6 cascade [28,100], we propose that the MPK3/MPK6 cascade is a key hub in orchestrating the trade-off between growth and defense.

MPK3/MPK6 activation-induced photosynthetic inhibition, as well as its associated ROS accumulation and HR cell death, contribute positively to the robust ETI. Regulation of photosynthetic inhibition by an active signaling cascade demonstrates that the inhibition of photosynthesis is an active defense response in plant immunity triggered by effectors, not a passive consequence of the deterioration of plant fitness caused by pathogen infection. It also reveals a potential mechanism underlying the growth–defense trade-off during plant immunity. Plant ETI is a stronger and more robust form of immune response in comparison to PTI [3,7,8]. In such a case, a robust defense, but not growth, is of high priority. Long-lasting activation of MPK3/MPK6 triggered by pathogen effectors contributes to the robustness of ETI (Fig 8G). It is worth noting that PTI, a weaker form of plant immunity, induces only transient MAPK activation and does not cause photosynthetic inhibition (Fig 3B and S4 Fig), indicating that photosynthetic activities are differently regulated during different forms of immune responses by the same MAPK signaling pathway, depending on its activation kinetics.

Materials and methods

Plant growth

Soil-grown *Arabidopsis* plants were maintained at 22 ˚C and about 70% relative humidity in a growth chamber with a 10 h day/14 h night cycle (100 μmol m^{-2} s^{-1}). For plants grown in liquid medium, seeds were surface sterilized. After stratification at 4 ˚C for 3–5 d, seeds were sown in petri dishes with liquid half-strength Murashige and Skoog medium and grown in a growth chamber at 22 ˚C with continuous light (70 μmol m^{-2} s^{-1}). Six-d-old seedlings were transferred to 20-mL GC vials with 6 mL of liquid half-strength MS medium (10 seedlings per vial) and maintained under the same growth conditions [25]. Col-0 ecotype was used as the wild type. Mutant alleles and transgenic lines of *mpk3-1* (Salk_151594), *mpk6-2* (Salk_073907), *DD* (*GVG-NtMEK2^{DD}*), *AvrRpt2/RPS2* (*GVG-AvrRpt2* in Col-0 background), *AvrRps2/rps2* (*GVG-AvrRpt2* in *rps2-101C* background), *MPK6SR* (*mpk3 mpk6 P$_{MPK6}$:MPK6^{YG}*, Line #58), and *MPK3SR* (*mpk3 mpk6 P$_{MPK3}$:MPK3^{TG}*, Line #64) were reported previously [52,65,101].

Generation of transgenic lines

For generation of *DD/pFld* and *GVG-AvrRpt2/pFld* plants, the coding sequence of *Fld* from cyanobacterium *Anabaena sp.* PCC 7119 [102] was first optimized to codons preferred in *Arabidopsis* using OptimumGene algorithm (Genscript) (S9 Fig). After introducing *Nde* I and *Spe* I enzyme digestion sites, the *Nde* I-*Fld*-*Spe* I fragment was directly synthesized into *pUC57* vector, and then the *Nde* I-*Fld*-*Spe* I fragment was subcloned into *pBluescript* (*pBS*) vectors with RbcS signal peptide sequence to generate *pBS-RbcS-Fld*. The *pBS-RbcS-Fld* was cut with *Xho* I and *Spe* I and subcloned into *pBID* vector to generate *pBID-RbcS-Fld* constructs. The

pBID-RbcS-Fld construct was then transformed to *Agrobacterium tumefaciens* GV3101. Finally, the *A. tumefaciens* GV3101 containing *pBID-RbcS-Fld* was used to transform *DD* and *GVG-AvrRpt2/RPS2* plants, respectively. Single insertion lines were selected and the expression of Fld was confirmed by immunoblot. F3 homozygous *DD/pFld* and *GVG-AvrRpt2/pFld* plants were used for experiments.

Chlorophyll fluorescence measurement

The O-J-I-P curve was measured by using Dual-PAM chlorophyll fluorometer (Walz, Germany) with a built-in fast kinetic protocol. Other chlorophyll fluorescence parameters were measured with the Maxi-version of Imaging-PAM chlorophyll fluorometer (Walz, Germany) or FMS2 (Hansatech, United Kingdom). F_o (minimum fluorescence of dark adapted leaves) was measured using weak light (<1 μmol m^{-2} s^{-1}) at a low frequency (2 Hz). For measuring F_m (maximum fluorescence yield of dark-adapted leaves), dark-adapted leaves were exposed to a PPFD of approximately 2,700 μmol m^{-2} s^{-1}. When performing induction kinetics measurements, the intensity of actinic light was set to 110 μmol m^{-2} s^{-1}. For NPQ induction analysis, the intensity of actinic light was set to 610 μmol m^{-2} s^{-1}. The interval for measuring Fm' (maximum fluorescence yield of light adapted leaves) was 20 s. Maximal PSII quantum yield (F_v/F_m) was calculated with $(F_m-F_o)/F_m$; effective quantum yield of PSII (Y(II)) with $(F_{m'}-F)/F_{m'}$; qL, the parameter estimating the open PSII centers based on a lake model, with $(F_m/F-F_m/F_{m'}) / (F_m/F_o -1)$; and NPQ, the nonphotochemical quenching parameter describing the regulated quenching of excessive energy, with $(F_m-F_{m'})/F_{m'}$.

ROS staining

In vivo H_2O_2 generation in plants was detected by using DAB as described previously [32]. Twelve-d-old *Arabidopsis* seedlings after treatment were submerged into a solution containing 1 mg/mL DAB (pH 5.5) for 2 h under growth light. Oxidation of DAB leads to its polymerization and deposition at the site of ROS generation. The seedlings were then boiled in ethanol for 10 min to remove chlorophyll. H_2O_2 production is visualized as a reddish-brown coloration. In vivo $O_2^{•-}$ production was monitored by NBT staining as described previously [32]. Twelve-d-old *Arabidopsis* seedlings after treatment were submerged into 10 mM potassium phosphate buffer (pH 7.8) containing 1 mg/mL NBT and 10 mM NaN_3. To avoid overstaining, the seedlings were stained in dark for 30 min. The seedlings were then boiled in ethanol for 10 min to remove chlorophyll. Reduced NBT was visualized as a dark blue-colored formazam deposit. Single layer mesophyll cells were prepared according to [103] for visualization of H_2O_2 and $O_2^{•-}$ accumulation in mesophyll cells. Seedlings stained with DAB and NBT were fixed in 3.5% glutaraldehyde for 1 h and then softened with 0.1 M EDTA, pH 9.0, for 2 h at 55 °C. A leaf sample (about 1 mm^2) was placed on a glass slide and covered with a cover slide. The leaf sample was stretched into a single cell layer by lightly tapping with the eraser of a pencil. H_2O_2 and $O_2^{•-}$ accumulation in chloroplasts were imaged with a microscope equipped with a digital camera.

Pathogen and ion leakage assay

HR assay was performed as described previously [104]. For HR assay in Col-0, *DD*, and *DD/pFld* plants, 4-wk-old plants were infiltrated with *Pst-AvrRpt2* (OD$_{600}$ = 0.02). For Col-0, *MPK6SR*, and *MPK3SR*, 4-wk-old plants were first sprayed with 10 μM NA-PP1 or DMSO (mock) 2 h before *Pst-AvrRpt2* (OD$_{600}$ = 0.02) infiltration. After infiltration, plants were kept under a growth light and HR phenotype was detected at 18 hpi. The disease resistance assay was carried out as previously described [25]. For the resistance assay in *DD* and *DD/pFld*,

4-wk-old plants were infiltrated with *Pst-AvrRpt2* (OD_{600} = 0.0005). For Col-0, *MPK6SR*, and *MPK3SR*, 4-wk-old plants were first sprayed with 10 μM NA-PP1 or DMSO (mock) 2 h before or at indicated times for *Pst-AvrRpt2* (OD_{600} = 0.0005), *Pst-AvrRpm1* (OD_{600} = 0.0005), *Pst-AvrB* (OD_{600} = 0.0005), and *Pst-AvrRps4* (OD_{600} = 0.0005) infiltration. Plants were maintained at 22 ˚C in a growth chamber with a 10 h day/14 h night cycle (100 μmol m^{-2} s^{-1}). Normally, for Col-0, *MPK6SR*, and *MPK3SR* were sprayed with 10 μM NA-PP1 or DMSO (mock) again at 1.5 dpi if not specified. Bacterial growth was quantified with 12 leaves (usually the fifth and sixth leaves) from 6 independent plants at 2.5 or 3 dpi.

Ion leakage assay was performed as previously described [105]. Plants were first sprayed with 10 μM NA-PP1 or DMSO (mock). Leaf discs (7 mm in diameter) were punched out and then vacuum infiltrated with *Pst-AvrRpt2* (OD_{600} = 0.02), *Pst-AvrRpm1* (OD_{600} = 0.02), *Pst-AvrB* (OD_{600} = 0.02), or *Pst-AvrRps4* (OD_{600} = 0.02). Leaf discs were then transferred to a 20-mL GC vial containing 10 mL ddH$_2$O with 2 μM NA-PP1 or DMSO (mock). Conductivity was measured by using a conductivity meter.

BN-PAGE and two-dimensional SDS-PAGE

Photosynthetic complexes were separated by BN-PAGE according to the modified protocol [106]. Twelve-d-old *Arabidopsis* seedlings grown in liquid medium were treated with 5 μM DEX for indicated time points. Seedlings (about 1.5 g) were ground in 10 mL thylakoid extraction buffer (50 mM HEPES/KOH, pH 7.5, 330 mM sorbitol, 2 mM EDTA, 1 mM MgCl$_2$, 5 mM ascorbate, 0.05% [w/v] BSA, and 10 mM NaF) and filtered through 4 layers of KimWipes. After centrifugation for 5 min at 4 ˚C, 2,500*g*, the pellet was successively washed with washing buffer I (50 mM HEPES/KOH, pH 7.5, 5 mM sorbitol, and 10 mM NaF) and washing buffer II (50 mM HEPES/KOH, pH 7.5, 100 mM sorbitol, 10 mM MgCl$_2$, and 10 mM NaF) at 2,500*g* for 5 min at 4 ˚C. Chlorophyll was extracted in 80% (v/v) buffered acetone (2.5 mM HEPES/ NaOH, pH 7.5) and the content of chlorophyll was determined according to the equation: Chlorophyll (μg/mL) = 20.2A_{645} + 8A_{663}. The thylakoid membrane was washed twice with a buffer (25 mM Bis Tris-HCl, pH 7.0, 20% [v/v] glycerol) at 12,000*g* for 5 min at 4 ˚C. Then, the thylakoids were solubilized in solubilization buffer (25 mM Bis Tris-HCl, pH 7.0, 20% [v/v] glycerol and 1% n-dodecyl-b-maltoside) for 10 min on ice. After solubilization, the samples were centrifuged at 12,000*g* for 10 min at 4 ˚C to remove insoluble ingredients. The supernatant was transferred to a new tube, and 1/10 volume of 10× native sample buffer (100 mM Bis Tris-HCl, pH 7.0, 0.5 M 6-amino-caproic acid, 30% [v/v] glycerol, and 0.5% [v/v] brilliant blue G-250) were added. Thylakoid membranes equivalent to 8 μg chlorophyll content were loaded to a 5%–13.5% gradient native PAGE gel and run at voltages of 50, 75, 100, 125, 150, 175, 200, 225, and 250 V, each for 0.5 h. After the first dimensional separation, strips were excised and incubated with 138 mM Tris/HCl, pH 6.8, 6 M urea, 22.2% (v/v) glycerol, 4.3% (w/v) SDS, and 5% (v/v) 2-mercaptoethanol for 1 h at room temperature. Then, the strips were loaded to a 15% (w/v) SDS-PAGE gel containing 6 M urea. Proteins on the 2D gels were visualized by staining with brilliant blue G-250.

Protein extraction and immunoblot analysis

Protein extraction and immunoblot were carried out as previously described [32]. Total protein was extracted from leaf tissue by grinding with small plastic pestles in extraction buffer (100 mM HEPES, pH 7.5, 5 mM EDTA, 5 mM EGTA, 10 mM DTT, 10 mM Na$_3$VO$_4$, 10 mM NaF, 50 mM b-glycerophosphate, 1 mM phenylmethylsulfonyl fluoride, 5 μg/mL antipain, 5 μg/mL aprotinin, 5 μg/mL leupeptin, and 10% [v/v] glycerol). Thylakoid proteins for immunoblot were prepared by adding 1/4 volume of 4× SDS sample buffer (250 mM Tris/HCl, pH

6.8, 40% [v/v] glycerol, 4% [w/v] SDS, and 0.1% [w/v] bromophenol blue) to solubilized thylakoid preparations and boiled for 2 min. NtMEK2^{DD} expression was detected by using anti-FLAG (Sigma, F1804, dilution 1:10,000). Activation of MPK3 and MPK6 was detected by using anti-pTEpY (Cell signaling, dilution 1:4,000). Expression of Fld was detected by anti-Fld (a gift from Dr. Donald A. Bryant, Pennsylvania State University, dilution 1:3,000). Anti-D1 antibody (Agrisera, AS10704, dilution 1:10,000) was used for the detection of PSII core D1 protein. The blots were incubated with horseradish peroxidase-conjugated goat-anti-mouse or goat-anti-rabbit secondary antibodies (dilution 1:10,000), and the bands were visualized using an enhanced chemiluminescence kit (Perkin Elmer) according to the manufacturer's instructions.

Quantitative RT-PCR analysis

Real-time quantitative PCR (qPCR) was performed as previously described [54]. Total RNA was extracted using TRizol reagent (Invitrogen). After DNase treatment, 1 μg of total RNA was used for reverse transcription. Real-time qPCR analysis was performed using an ABI 7500 real-time PCR machine (Life Technologies). *EF-1a* was used as an internal control. The primer pairs used for qPCR are listed in S2 Table.

Illumina RNA-seq gene expression profiling

Total RNA was extracted with TRizol reagent (Invitrogen) from 12-d-old *DD* seedlings treated with 2 μM DEX for 0 and 6 h, respectively. After DNase treatment, total RNA was purified using RNA clean and concentrator Kit. RNA sequencing libraries were constructed using TruSeq RNA library preparation Kit and sequenced using the HiSeq X Ten according to the manufacturer's instructions. Dirty raw reads were filtered out using SONPnuke software. Clean reads were mapped to the *Arabidopsis* reference genome with BWA and to reference gene sequences with Bowtie. Gene expression levels were calculated using the RPKM method (reads per kb per million reads). The raw Illumina reads generated from RNA-seq experiments were deposited at NCBI Sequence Read Archive (SRP111959).

Quantification and statistical analysis

Statistical details of experiments are reported in figure legends. Statistical significance between groups was determined by one-way ANOVA comparison; *p*-values were indicated in figure legends. Each experiment was performed at least twice, with similar results.

Supporting information

S1 Fig. Activation of MPK3/MPK6 causes disassembly of photosynthetic complexes, related to Fig 2. Activation of MPK3/MPK6 causes disassembly of PSII-LHCII super-complexes and accumulation of the intermediate CP43-less PSII core complex. Twelve-d-old *DD* plants grown in liquid medium were treated with 5 μM DEX for indicated periods of time. Thylakoid membrane samples equivalent to 8 μg of chlorophyll content were subjected to first dimension BN-PAGE. The BN-PAGE strips were cut out. After denaturation, the samples were subjected to second dimension SDS-PAGE. Protein spots were visualized by brilliant blue G250 staining. Bands and protein spots were labeled as described previously. BN-PAGE, blue native polyacrylamide gel electrophoresis; CP43, photosystem II chlorophyll protein at 43 kDa; *DD*, *GVG-NtMEK2^{DD}*; DEX, dexamethasone; LHCII, light-harvesting complex II; mc, mega-complex; MPK, mitogen-activated protein kinase; PSII, photosystem II; sc, super-

complex; SDS-PAGE, sodium dodecyl sulfate-PAGE.
(TIF)

S2 Fig. Activation of MPK3/MPK6 causes ROS accumulation, related to Fig 2. Activation of MPK3/MPK6 leads to increases in H_2O_2 (**A**) and $O_2^{\bullet-}$ (**B**) levels in whole seedlings. *DD* plants grown in liquid medium were treated with EtOH or 5 μM DEX and were kept under light for indicated periods of time. H_2O_2 and $O_2^{\bullet-}$ were visualized by DAB and NBT staining, respectively. DAB, 3,3′-diaminobenzidine; *DD*, *GVG-NtMEK2^{DD}*; DEX, dexamethasone; EtOH, ethanol; MPK, mitogen-activated protein kinase; NBT, nitroblue tetrazolium; ROS, reactive oxygen species.
(TIF)

S3 Fig. Transient activation of MPK3/MPK6 after flg22 treatment does not induce a decrease in PSII core D1 protein, related to Fig 3. Twelve-d-old *DD* and Col-0 plants grown in liquid medium were treated with 5 μM DEX and 200 nM flg22 for indicated times, respectively. Thylakoid membranes were isolated and solubilized with 1% dodecyl maltoside. Samples equivalent to 8 μg of chlorophyll were loaded to a BN-PAGE. For detection of D1 abundance in different complexes, samples equivalent to 2 μg of chlorophyll were loaded to a BN-PAGE. After transferring to a PVDF membrane, anti-D1 was used to detect D1 abundance. BN-PAGE, blue native polyacrylamide gel electrophoresis; Col-0, Columbia-0; DEX, dexamethasone; flg22, a 22 amino acids flagellin fragment; MPK, mitogen-activated protein kinase; PSII, photosystem II; PVDF, polyvinylidene fluoride.
(TIF)

S4 Fig. ETI is associated with photosynthetic inhibition, related to Fig 4. (**A** and **B**) Photosynthetic parameters are differentially affected by different *Pst* strains. Four-wk-old Col-0 plants were infiltrated with 10 mM $MgCl_2$ (mock), *Pst-EV*, *Pst-AvrRpt2*, or *Pst-hrcC⁻* (OD_{600} = 0.2). The plants were covered with a transparent lid (100% relative humidity) and kept under light. Fv/Fm and Y(II) were measured at the indicated time. Values are means ± SD, *n* = 8. (**C**) Flg22-triggered PTI does not induce photosynthetic inhibition. Four-wk-old Col-0 plants were infiltrated with 10 mM $MgCl_2$ (mock) or 50 nM flg22. Photosynthetic parameters were measured at 24 hpi. Values are means ± SD, *n* = 8. (**D** and **E**) AvrRpm1-triggered ETI also induces photosynthetic inhibition. Four-wk-old Col-0 plants were infiltrated with 10 mM $MgCl_2$ (mock), *P. fluorescens-EV* (*Pf0-1-EV*), or *P. fluorescens-AvrRpm1* (*Pf0-1-AvrRpm1*) (OD_{600} = 0.02). Fv/Fm and Y(II) were measured at indicated time points. Values are means ± SD, *n* = 8. The numerical values used to construct panels A–E can be found in S1 Data. AvrRpm1, avirulence effector recognized by RPM1; *AvrRpt2*, avirulence effector recognized by RPS2; Col-0, Columbia-0; ETI, effector-triggered immunity; *EV*, empty vector; flg22, a 22 amino acids flagellin fragment; hpi, hours post inoculation; *hrcC⁻*, outer membrane type III secretion protein HrcC mutant; OD, optical density; *Pf0-1-AvrRpm1*, *P. fluorescens-AvrRpm1*; *Pf0-1-EV*, *P. fluorescens-EV*; *Pst*, *Pseudomonas syringae* pv *tomato*; PTI, PAMP-triggered immunity.
(TIF)

S5 Fig. ETI causes ROS accumulation in chloroplast, related to Fig 4. AvrRpt2-mediated ETI results in light-dependent increases in $O_2^{\bullet-}$ and H_2O_2 production in chloroplasts. Twelve-d-old *GVG-AvrRpt2/RPS2* and *GVG-AvrRpt2/rps2* plants were treated with DEX (5 μM) or EtOH solvent control for 8 h. $O_2^{\bullet-}$ and H_2O_2 accumulation was detected by NBT (**A**) and DAB (**B**) staining, respectively. Images of ROS accumulation at whole leaf level and subcellular level were shown. AvrRpt2, avirulence effector recognized by RPS2; DAB, 3,3′-diaminobenzidine; DEX, dexamethasone; ETI, effector-triggered immunity; EtOH, ethanol; *GVG-AvrRpt2*, DEX-

inducible promoter-driven *AvrRpt2*; NBT, nitroblue tetrazolium; $O_2^{\bullet-}$, superoxide; ROS, reactive oxygen species; *RPS2*, Resistance to *Pseudomonas syringae* 2.
(TIF)

S6 Fig. MPK3 and MPK6 are required for both CNL and TNL NLR-mediated ETI, related to Fig 5. (**A**) Four-wk-old plants were first sprayed with DMSO or 10 μM NA-PP1 for 2 h before infiltration with *Pst-AvrRpm1* (OD$_{600}$ = 0.0005), *Pst-AvrB* (OD$_{600}$ = 0.0005), or *Pst-AvrRps4* (OD$_{600}$ = 0.0005). NA-PP1 or DMSO was sprayed again at 1.5 dpi. *Pst-AvrRpt2* growth was quantified at 3 dpi. Values are means ± SD, *n* = 3, *P ≤ 0.001. (**B**) Plants pretreated with DMSO or 10 μM NA-PP1 were infiltrated with *Pst-AvrRpm1* (OD$_{600}$ = 0.02), *Pst-AvrB* (OD$_{600}$ = 0.02), or *Pst-AvrRps4* (OD$_{600}$ = 0.02). Soil-grown Col-0, *MPK6SR*, and *MPK3SR* plants were first spray treated with 10 μM NA-PP1 for 2 h, and leaf discs were punched and then infiltrated with *Pst-AvrRpt2* (OD = 0.02) by vacuum. Leaf discs were then transferred to GC vials containing 2 μM NA-PP1 or DMSO. Ion leakage was measured as increase in conductivity. Values are means ± SD, *n* = 3. (**C**) Four-wk-old soil-grown Col-0, *MPK6SR*, and *MPK3SR* plants were first spray treated with NA-PP1 (10 μM) or DMSO solvent control for 2 h and then infiltrated with *Pst-AvrRpm1* (OD = 0.02), *Pst-AvrB* (OD = 0.02), and *Pst-AvrRps4* (OD = 0.02). Values are means ± SD, *n* = 8. The numerical values used to construct panels A–C can be found in S1 Data. *AvrB*, avirulence protein B; *AvrRpm1*, avirulence effector recognized by RPM1; *AvrRps4*, avirulence effector recognized by RPS4; CNL, coiled coil-nucleotide binding site-leucine rich repeat; Col-0, Columbia-0; ETI, effector-triggered immunity; GC, gas chromatography; MPK, mitogen-activated protein kinase; NA-PP1, 4-amino-1-tert-butyl-3-(1'-naphthyl)pyrazolo[3,4-d]pyrimidine; NLR, nucleotide-binding leucine-rich repeat; OD, optical density; *Pst*, *Pseudomonas syringae* pv *tomato*; TNL, toll/interleukin-1 receptor-nucleotide binding site-leucine rich repeat.
(TIF)

S7 Fig. Expression of pFld impairs AvrRpt2-induced PSII inhibition, related to Fig 7. (**A**) Expression of pFld causes growth retardation. Four-wk-old soil-grown *pFld* transgenic plants in *GVG-AvrRpt2* background were shown. (**B**) Immunoblot analysis of Fld expression in *pFld* transgenic plants using anti-Fld antibody. (**C**) AvrRpt2-induced PSII inactivation is delayed in *pFld* transgenic lines. Twelve-d-old *GVG-AvrRpt2*, *GVG-AvrRpt2/pFld-4*, and *GVG-AvrRpt2/pFld-34* plants grown in liquid medium were treated with EtOH or 5 μM DEX. Fv/Fm was measured at 18 hpi. Values are means ± SD, *n* = 6, **P ≤ 0.001. The numerical values used to construct panel C can be found in S1 Data. AvrRpt2, avirulence effector recognized by RPS2; DEX, dexamethasone; EtOH, ethanol; Fld, flavodoxin; *GVG-AvrRpt2*, DEX-inducible promoter-driven *AvrRpt2*; hpi, hours post inoculation; pFld, plastid-targeted cyanobacterial flavodoxin; PSII, photosystem II.
(TIF)

S8 Fig. Expression of pFld impairs AvrRpt2-induced PSII inhibition, related to Fig 8. Twelve-d-old *DD* and *DD pFld* plants grown in liquid medium were treated with *Pst-AvrRpt2* (OD = 0.02); disassembly of photosynthetic complexes at 24 hpi was visualized with BN-PAGE. Thylakoid membranes were isolated and solubilized with 1% dodecyl maltoside. Samples equivalent to 8 μg of chlorophyll were loaded to a blue native polyacrylamide gel (BN-PAGE). AvrRpt2, avirulence effector recognized by RPS2; BN-PAGE, blue native polyacrylamide gel electrophoresis; *DD*, *GVG-NtMEK2^{DD}*; hpi, hours post inoculation; OD, optical density; pFLD; plastid-targeted cyanobacterial flavodoxin; PSII, photosystem II; *Pst*, *Pseudomonas syringae* pv *tomato*.
(TIF)

S9 Fig. Original and optimized sequence for Fld. The coding sequence of *Fld* from cyanobacterium *Anabaena sp*. PCC 7119 was optimized using OptimumGene algorithm (Genscript, http://www.genscript.com). *Fld*, flavodoxin.
(TIF)

S1 Table. List of MPK3/MPK6 activation-regulated genes. MPK, mitogen-activated protein kinase.
(XLSX)

S2 Table. Primers used in this study.
(XLSX)

S1 Data. Numerical values for bar and line charts in this study.
(XLSX)

Acknowledgments

Author Contributions

Conceptualization: Jianbin Su, Shuqun Zhang.

Data curation: Jianbin Su, Liuyi Yang, Qiankun Zhu, Hongjiao Wu, Yi He, Yidong Liu, Juan Xu.

Formal analysis: Jianbin Su.

Investigation: Jianbin Su, Liuyi Yang, Qiankun Zhu, Hongjiao Wu, Yi He, Yidong Liu.

Methodology: Jianbin Su, Liuyi Yang.

Project administration: Shuqun Zhang.

Resources: Dean Jiang, Shuqun Zhang.

Supervision: Shuqun Zhang.

Validation: Jianbin Su, Juan Xu.

Writing – original draft: Jianbin Su, Shuqun Zhang.

Writing – review & editing: Shuqun Zhang.

References

1. Ausubel FM. Are innate immune signaling pathways in plants and animals conserved? Nat Immunol. 2005; 6: 973–979. https://doi.org/10.1038/ni1253 PMID: 16177805

2. Boller T, He SY. Innate immunity in plants: an arms race between pattern recognition receptors in plants and effectors in microbial pathogens. Science. 2009; 324: 742–744. https://doi.org/10.1126/science.1171647 PMID: 19423812

3. Jones JD, Dangl JL. The plant immune system. Nature. 2006; 444: 323–329. https://doi.org/10.1038/nature05286 PMID: 17108957

4. Spoel SH, Dong X. How do plants achieve immunity? Defence without specialized immune cells. Nat Rev Immunol. 2012; 12: 89–100. https://doi.org/10.1038/nri3141 PMID: 22273771

5. Zipfel C. Plant pattern-recognition receptors. Trends Immunol. 2014; 35: 345–351. https://doi.org/10.1016/j.it.2014.05.004 PMID: 24946686

6. Chisholm ST, Coaker G, Day B, Staskawicz BJ. Host-microbe interactions: shaping the evolution of the plant immune response. Cell. 2006; 124: 803–814. https://doi.org/10.1016/j.cell.2006.02.008 PMID: 16497589

7. Cui H, Tsuda K, Parker JE. Effector-triggered immunity: from pathogen perception to robust defense. Annu Rev Plant Biol. 2015; 66: 487–511. https://doi.org/10.1146/annurev-arplant-050213-040012 PMID: 25494461

8. Dodds PN, Rathjen JP. Plant immunity: towards an integrated view of plant-pathogen interactions. Nat Rev Genet. 2010; 11: 539–548. https://doi.org/10.1038/nrg2812 PMID: 20585331

9. Gassmann W, Bhattacharjee S. Effector-triggered immunity signaling: from gene-for-gene pathways to protein-protein interaction networks. Mol Plant Microbe Interact. 2012; 25: 862–868. https://doi.org/10.1094/MPMI-01-12-0024-IA PMID: 22414439

10. Glazebrook J. Contrasting mechanisms of defense against biotrophic and necrotrophic pathogens. Annu Rev Phytopathol. 2005; 43: 205–227. https://doi.org/10.1146/annurev.phyto.43.040204.135923 PMID: 16078883

11. Yu X, Feng B, He P, Shan L. From chaos to harmony: Responses and signaling upon microbial pattern recognition. Annu Rev Phytopathol. 2017; 55: 109–137. https://doi.org/10.1146/annurev-phyto-080516-035649 PMID: 28525309

12. Peng Y, Wersch RV, Zhang Y. Convergent and divergent signaling in PAMP-triggered immunity and effector-triggered immunity. Mol Plant Microbe Interact. 2017.

13. Su J, Spears BJ, Kim SH, Gassmann W. Constant vigilance: plant functions guarded by resistance proteins. Plant J. 2017.

14. Qi D, Innes RW. Recent advances in plant NLR structure, function, localization, and signaling. Front Immunol. 2013; 4: 348. https://doi.org/10.3389/fimmu.2013.00348 PMID: 24155748

15. Jones JD, Vance RE, Dangl JL. Intracellular innate immune surveillance devices in plants and animals. Science. 2016; 354: aaf6395.

16. Baggs E, Dagdas G, Krasileva KV. NLR diversity, helpers and integrated domains: making sense of the NLR IDentity. Curr Opin Plant Biol. 2017; 38: 59–67. https://doi.org/10.1016/j.pbi.2017.04.012 PMID: 28494248

17. Bentham A, Burdett H, Anderson PA, Williams SJ, Kobe B. Animal NLRs provide structural insights into plant NLR function. Ann Bot. 2017; 119: 827–702. https://doi.org/10.1093/aob/mcw171 PMID: 27562749

18. van der Hoorn RA, Kamoun S. From Guard to Decoy: a new model for perception of plant pathogen effectors. Plant Cell. 2008; 20: 2009–2017. https://doi.org/10.1105/tpc.108.060194 PMID: 18723576

19. Dangl JL, Horvath DM, Staskawicz BJ. Pivoting the plant immune system from dissection to deployment. Science. 2013; 341: 746–751. https://doi.org/10.1126/science.1236011 PMID: 23950531

20. Cesari S, Bernoux M, Moncuquet P, Kroj T, Dodds PN. A novel conserved mechanism for plant NLR protein pairs: the "integrated decoy" hypothesis. Front Plant Sci. 2014; 5: 606. https://doi.org/10.3389/fpls.2014.00606 PMID: 25506347

21. Bigeard J, Colcombet J, Hirt H. Signaling mechanisms in pattern-triggered immunity (PTI). Mol Plant. 2015; 8: 521–539. https://doi.org/10.1016/j.molp.2014.12.022 PMID: 25744358

22. Coll NS, Epple P, Dangl JL. Programmed cell death in the plant immune system. Cell Death Differ. 2011; 18: 1247–1256. https://doi.org/10.1038/cdd.2011.37 PMID: 21475301

23. Gao X, Chen X, Lin W, Chen S, Lu D, Niu Y, et al. Bifurcation of Arabidopsis NLR immune signaling via Ca2+-dependent protein kinases. PLoS Pathog. 2013; 9: e1003127. https://doi.org/10.1371/journal.ppat.1003127 PMID: 23382673

24. Tsuda K, Mine A, Bethke G, Igarashi D, Botanga CJ, Tsuda Y, et al. Dual regulation of gene expression mediated by extended MAPK activation and salicylic acid contributes to robust innate immunity in Arabidopsis thaliana. PLoS Genet. 2013; 9: e1004015. https://doi.org/10.1371/journal.pgen.1004015 PMID: 24348271

25. Guan R, Su J, Meng X, Li S, Liu Y, Xu J, et al. Multilayered regulation of ethylene induction plays a positive role in Arabidopsis resistance against Pseudomonas syringae. Plant Physiol. 2015; 169: 299–312. https://doi.org/10.1104/pp.15.00659 PMID: 26265775

26. Nomura H, Komori T, Uemura S, Kanda Y, Shimotani K, Nakai K, et al. Chloroplast-mediated activation of plant immune signalling in Arabidopsis. Nat Commun. 2012; 3: 926. https://doi.org/10.1038/ncomms1926 PMID: 22735454

27. Couto D, Zipfel C. Regulation of pattern recognition receptor signalling in plants. Nat Rev Immunol. 2016; 16: 537–552. https://doi.org/10.1038/nri.2016.77 PMID: 27477127

28. Meng X, Zhang S. MAPK cascades in plant disease resistance signaling. Annu Rev Phytopathol. 2013; 51: 245–266. https://doi.org/10.1146/annurev-phyto-082712-102314 PMID: 23663002

29. Cui H, Gobbato E, Kracher B, Qiu J, Bautor J, Parker JE. A core function of EDS1 with PAD4 is to protect the salicylic acid defense sector in Arabidopsis immunity. New Phytol. 2017; 213: 1802–1817. https://doi.org/10.1111/nph.14302 PMID: 27861989

30. Wang S, Gu Y, Zebell SG, Anderson LK, Wang W, Mohan R, et al. A noncanonical role for the CKI-RB-E2F cell-cycle signaling pathway in plant effector-triggered immunity. Cell Host Microbe. 2014; 16: 787–794. https://doi.org/10.1016/j.chom.2014.10.005 PMID: 25455564

31. Caplan JL, Kumar AS, Park E, Padmanabhan MS, Hoban K, Modla S, et al. Chloroplast stromules function during innate immunity. Dev Cell. 2015; 34: 45–57. https://doi.org/10.1016/j.devcel.2015.05.011 PMID: 26120031

32. Liu Y, Ren D, Pike S, Pallardy S, Gassmann W, Zhang S. Chloroplast-generated reactive oxygen species are involved in hypersensitive response-like cell death mediated by a mitogen-activated protein kinase cascade. Plant J. 2007; 51: 941–954. https://doi.org/10.1111/j.1365-313X.2007.03191.x PMID: 17651371

33. Zurbriggen MD, Carrillo N, Tognetti VB, Melzer M, Peisker M, Hause B, et al. Chloroplast-generated reactive oxygen species play a major role in localized cell death during the non-host interaction between tobacco and Xanthomonas campestris pv. vesicatoria. Plant J. 2009; 60: 962–973. https://doi.org/10.1111/j.1365-313X.2009.04010.x PMID: 19719480

34. Heidrich K, Wirthmueller L, Tasset C, Pouzet C, Deslandes L, Parker JE. Arabidopsis EDS1 connects pathogen effector recognition to cell compartment-specific immune responses. Science. 2011; 334: 1401–1404. https://doi.org/10.1126/science.1211641 PMID: 22158818

35. Bethke G, Pecher P, Eschen-Lippold L, Tsuda K, Katagiri F, Glazebrook J, et al. Activation of the Arabidopsis thaliana mitogen-activated protein kinase MPK11 by the flagellin-derived elicitor peptide, flg22. Mol Plant Microbe Interact. 2012; 25: 471–480. https://doi.org/10.1094/MPMI-11-11-0281 PMID: 22204645

36. Pitzschke A, Schikora A, Hirt H. MAPK cascade signalling networks in plant defence. Curr Opin Plant Biol. 2009; 12: 421–426. https://doi.org/10.1016/j.pbi.2009.06.008 PMID: 19608449

37. Rasmussen MW, Roux M, Petersen M, Mundy J. MAP Kinase Cascades in Arabidopsis Innate Immunity. Front Plant Sci. 2012; 3: 169. https://doi.org/10.3389/fpls.2012.00169 PMID: 22837762

38. Su J, Zhang M, Zhang L, Sun T, Liu Y, Lukowitz W, et al. Regulation of stomatal immunity by interdependent functions of a pathogen-responsive MPK3/MPK6 cascade and abscisic acid. Plant Cell. 2017; 29: 526–542. https://doi.org/10.1105/tpc.16.00577 PMID: 28254778

39. Tena G, Asai T, Chiu WL, Sheen J. Plant mitogen-activated protein kinase signaling cascades. Curr Opin Plant Biol. 2001; 4: 392–400. PMID: 11597496

40. Pedley KF, Martin GB. Role of mitogen-activated protein kinases in plant immunity. Curr Opin Plant Biol. 2005; 8: 541–547. https://doi.org/10.1016/j.pbi.2005.07.006 PMID: 16043387

41. Ballare CL. Light regulation of plant defense. Annu Rev Plant Biol. 2014; 65: 335–363. https://doi.org/10.1146/annurev-arplant-050213-040145 PMID: 24471835

42. Stael S, Kmiecik P, Willems P, Van Der Kelen K, Coll NS, Teige M, et al. Plant innate immunity—sunny side up? Trends Plant Sci. 2015; 20: 3–11. https://doi.org/10.1016/j.tplants.2014.10.002 PMID: 25457110

43. Roden LC, Ingle RA. Lights, rhythms, infection: the role of light and the circadian clock in determining the outcome of plant-pathogen interactions. Plant Cell. 2009; 21: 2546–2552. https://doi.org/10.1105/tpc.109.069922 PMID: 19789275

44. Bilgin DD, Zavala JA, Zhu J, Clough SJ, Ort DR, DeLucia EH. Biotic stress globally downregulates photosynthesis genes. Plant Cell Environ. 2010; 33: 1597–1613. https://doi.org/10.1111/j.1365-3040.2010.02167.x PMID: 20444224

45. Bonfig KB, Schreiber U, Gabler A, Roitsch T, Berger S. Infection with virulent and avirulent P. syringae strains differentially affects photosynthesis and sink metabolism in Arabidopsis leaves. Planta. 2006; 225: 1–12. https://doi.org/10.1007/s00425-006-0303-3 PMID: 16807755

46. Berger S, Benediktyova Z, Matous K, Bonfig K, Mueller MJ, Nedbal L, et al. Visualization of dynamics of plant-pathogen interaction by novel combination of chlorophyll fluorescence imaging and statistical analysis: differential effects of virulent and avirulent strains of P. syringae and of oxylipins on A. thaliana. J Exp Bot. 2007; 58: 797–806. https://doi.org/10.1093/jxb/erl208 PMID: 17138624

47. de Torres Zabala M, Littlejohn G, Jayaraman S, Studholme D, Bailey T, Lawson T, et al. Chloroplasts play a central role in plant defence and are targeted by pathogen effectors. Nat Plants. 2015; 1: 15074. https://doi.org/10.1038/nplants.2015.74 PMID: 27250009

48. Yang C, Zhang Z, Gao H, Liu M, Fan X. Mechanisms by which the infection of Sclerotinia sclerotiorum (Lib.) de Bary affects the photosynthetic performance in tobacco leaves. BMC Plant Biol. 2014; 14: 240. https://doi.org/10.1186/s12870-014-0240-4 PMID: 25246003

49. Hodgson RA, Beachy RN, Pakrasi HB. Selective inhibition of photosystem II in spinach by tobacco mosaic virus: an effect of the viral coat protein. FEBS Lett. 1989; 245: 267–270. PMID: 2924924

50. Lehto K, Tikkanen M, Hiriart JB, Paakkarinen V, Aro EM. Depletion of the photosystem II core complex in mature tobacco leaves infected by the flavum strain of tobacco mosaic virus. Mol Plant Microbe Interact. 2003; 16: 1135–1144. https://doi.org/10.1094/MPMI.2003.16.12.1135 PMID: 14651347

51. Gururani MA, Venkatesh J, Tran LP. Regulation of photosynthesis during abiotic stress-induced photoinhibition. Mol Plant. 2015; 8: 1304–1320. https://doi.org/10.1016/j.molp.2015.05.005 PMID: 25997389

52. Ren D, Yang H, Zhang S. Cell death mediated by MAPK is associated with hydrogen peroxide production in Arabidopsis. J Biol Chem. 2002; 277: 559–565. https://doi.org/10.1074/jbc.M109495200 PMID: 11687590

53. Ren D, Liu Y, Yang KY, Han L, Mao G, Glazebrook J, et al. A fungal-responsive MAPK cascade regulates phytoalexin biosynthesis in Arabidopsis. Proc Natl Acad Sci USA. 2008; 105: 5638–5643. https://doi.org/10.1073/pnas.0711301105 PMID: 18378893

54. Mao G, Meng X, Liu Y, Zheng Z, Chen Z, Zhang S. Phosphorylation of a WRKY transcription factor by two pathogen-responsive MAPKs drives phytoalexin biosynthesis in Arabidopsis. Plant Cell. 2011; 23: 1639–1653. https://doi.org/10.1105/tpc.111.084996 PMID: 21498677

55. Meng X, Xu J, He Y, Yang KY, Mordorski B, Liu Y, et al. Phosphorylation of an ERF transcription factor by Arabidopsis MPK3/MPK6 regulates plant defense gene induction and fungal resistance. Plant Cell. 2013; 25: 1126–1142. https://doi.org/10.1105/tpc.112.109074 PMID: 23524660

56. Xu J, Meng J, Meng X, Zhao Y, Liu J, Sun T, et al. Pathogen-responsive MPK3 and MPK6 reprogram the biosynthesis of indole glucosinolates and their derivatives in Arabidopsis immunity. Plant Cell. 2016; 28: 1144–1162. https://doi.org/10.1105/tpc.15.00871 PMID: 27081184

57. Huang da W, Sherman BT, Lempicki RA. Bioinformatics enrichment tools: paths toward the comprehensive functional analysis of large gene lists. Nucleic Acids Res. 2009; 37: 1–13. https://doi.org/10.1093/nar/gkn923 PMID: 19033363

58. Huang da W, Sherman BT, Lempicki RA. Systematic and integrative analysis of large gene lists using DAVID bioinformatics resources. Nat Protoc. 2009; 4: 44–57. https://doi.org/10.1038/nprot.2008.211 PMID: 19131956

59. Baker NR. Chlorophyll fluorescence: a probe of photosynthesis in vivo. Annu Rev Plant Biol. 2008; 59: 89–113. https://doi.org/10.1146/annurev.arplant.59.032607.092759 PMID: 18444897

60. Stirbet A, Riznichenko GY, Rubin AB, Govindjee. Modeling chlorophyll a fluorescence transient: relation to photosynthesis. Biochemistry. 2014; 79: 291–323. https://doi.org/10.1134/S0006297914040014 PMID: 24910205

61. Muller P, Li XP, Niyogi KK. Non-photochemical quenching. A response to excess light energy. Plant Physiol. 2001; 125: 1558–1566. PMID: 11299337

62. Lambrev PH, Miloslavina Y, Jahns P, Holzwarth AR. On the relationship between non-photochemical quenching and photoprotection of Photosystem II. Biochimi Biophys Acta. 2012; 1817: 760–769.

63. Kato Y, Miura E, Ido K, Ifuku K, Sakamoto W. The variegated mutants lacking chloroplastic FtsHs are defective in D1 degradation and accumulate reactive oxygen species. Plant Physiol. 2009; 151: 1790–1801. https://doi.org/10.1104/pp.109.146589 PMID: 19767385

64. Lu Y, Hall DA, Last RL. A small zinc finger thylakoid protein plays a role in maintenance of photosystem II in Arabidopsis thaliana. Plant Cell. 2011; 23: 1861–1875. https://doi.org/10.1105/tpc.111.085456 PMID: 21586683

65. Xu J, Xie J, Yan C, Zou X, Ren D, Zhang S. A chemical genetic approach demonstrates that MPK3/MPK6 activation and NADPH oxidase-mediated oxidative burst are two independent signaling events in plant immunity. Plant J. 2014; 77: 222–234. https://doi.org/10.1111/tpj.12382 PMID: 24245741

66. Thomas WJ, Thireault CA, Kimbrel JA, Chang JH. Recombineering and stable integration of the Pseudomonas syringae pv. syringae 61 hrp/hrc cluster into the genome of the soil bacterium Pseudomonas fluorescens Pf0-1. Plant J. 2009; 60: 919–928. https://doi.org/10.1111/j.1365-313X.2009.03998.x PMID: 19682294

67. McNellis TW, Mudgett MB, Li K, Aoyama T, Horvath D, Chua NH, et al. Glucocorticoid-inducible expression of a bacterial avirulence gene in transgenic Arabidopsis induces hypersensitive cell death. Plant J. 1998; 14: 247–257. PMID: 9628020

68. Mackey D, Belkhadir Y, Alonso JM, Ecker JR, Dangl JL. Arabidopsis RIN4 is a target of the type III virulence effector AvrRpt2 and modulates RPS2-mediated resistance. Cell. 2003; 112: 379–389. PMID: 12581527

69. Axtell MJ, Staskawicz BJ. Initiation of RPS2-specified disease resistance in Arabidopsis is coupled to the AvrRpt2-directed elimination of RIN4. Cell. 2003; 112: 369–377. PMID: 12581526

70. Mackey D, Holt BF 3rd, Wiig A, Dangl JL. RIN4 interacts with Pseudomonas syringae type III effector molecules and is required for RPM1-mediated resistance in Arabidopsis. Cell. 2002; 108: 743–754. PMID: 11955429

71. Bent AF, Kunkel BN, Dahlbeck D, Brown KL, Schmidt R, Giraudat J, et al. RPS2 of Arabidopsis thaliana: a leucine-rich repeat class of plant disease resistance genes. Science. 1994; 265: 1856–1860. PMID: 8091210

72. Grant MR, Godiard L, Straube E, Ashfield T, Lewald J, Sattler A, et al. Structure of the Arabidopsis RPM1 gene enabling dual specificity disease resistance. Science. 1995; 269: 843–846. PMID: 7638602

73. Eitas TK, Nimchuk ZL, Dangl JL. Arabidopsis TAO1 is a TIR-NB-LRR protein that contributes to disease resistance induced by the Pseudomonas syringae effector AvrB. Proc Natl Acad Sci USA. 2008; 105: 6475–6480. https://doi.org/10.1073/pnas.0802157105 PMID: 18424557

74. Gassmann W, Hinsch ME, Staskawicz BJ. The Arabidopsis RPS4 bacterial-resistance gene is a member of the TIR-NBS-LRR family of disease-resistance genes. Plant J. 1999; 20: 265–277. PMID: 10571887

75. Hinsch M, Staskawicz B. Identification of a new Arabidopsis disease resistance locus, RPs4, and cloning of the corresponding avirulence gene, avrRps4, from Pseudomonas syringae pv. pisi. Mol Plant Microbe Interact. 1996; 9: 55–61. PMID: 8589423

76. Yang KY, Liu Y, Zhang S. Activation of a mitogen-activated protein kinase pathway is involved in disease resistance in tobacco. Proc Natl Acad Sci USA. 2001; 98: 741–746. https://doi.org/10.1073/pnas.98.2.741 PMID: 11209069

77. del Pozo O, Pedley KF, Martin GB. MAPKKKα is a positive regulator of cell death associated with both plant immunity and disease. EMBO J. 2004; 23: 3072–3082. https://doi.org/10.1038/sj.emboj.7600283 PMID: 15272302

78. Pierella Karlusich JJ, Lodeyro AF, Carrillo N. The long goodbye: the rise and fall of flavodoxin during plant evolution. J Exp Bot. 2014; 65: 5161–5178. https://doi.org/10.1093/jxb/eru273 PMID: 25009172

79. Tognetti VB, Zurbriggen MD, Morandi EN, Fillat MF, Valle EM, Hajirezaei MR, et al. Enhanced plant tolerance to iron starvation by functional substitution of chloroplast ferredoxin with a bacterial flavodoxin. Proc Natl Acad Sci USA. 2007; 104: 11495–11500. https://doi.org/10.1073/pnas.0704553104 PMID: 17592141

80. Tognetti VB, Palatnik JF, Fillat MF, Melzer M, Hajirezaei MR, Valle EM, et al. Functional replacement of ferredoxin by a cyanobacterial flavodoxin in tobacco confers broad-range stress tolerance. Plant Cell. 2006; 18: 2035–2050. https://doi.org/10.1105/tpc.106.042424 PMID: 16829589

81. Goni G, Herguedas B, Hervas M, Peregrina JR, De la Rosa MA, Gomez-Moreno C, et al. Flavodoxin: a compromise between efficiency and versatility in the electron transfer from Photosystem I to Ferredoxin-NADP(+) reductase. Biochim Biophys Acta. 2009; 1787: 144–154. https://doi.org/10.1016/j.bbabio.2008.12.006 PMID: 19150326

82. Krieger-Liszkay A, Kos PB, Hideg E. Superoxide anion radicals generated by methylviologen in photosystem I damage photosystem II. Physiol Plant. 2011; 142: 17–25. https://doi.org/10.1111/j.1399-3054.2010.01416.x PMID: 20875060

83. Song YG, Liu B, Wang LF, Li MH, Liu Y. Damage to the oxygen-evolving complex by superoxide anion, hydrogen peroxide, and hydroxyl radical in photoinhibition of photosystem II. Photosynth Res. 2006; 90: 67–78. https://doi.org/10.1007/s11120-006-9111-7 PMID: 17131094

84. Yamashita A, Nijo N, Pospisil P, Morita N, Takenaka D, Aminaka R, et al. Quality control of photosystem II: reactive oxygen species are responsible for the damage to photosystem II under moderate heat stress. J Biol Chem. 2008; 283: 28380–28391. https://doi.org/10.1074/jbc.M710465200 PMID: 18664569

85. Bhattacharyya D, Gnanasekaran P, Kumar RK, Kushwaha NK, Sharma VK, Yusuf MA, et al. A geminivirus betasatellite damages the structural and functional integrity of chloroplasts leading to symptom formation and inhibition of photosynthesis. J Exp Bot. 2015; 66: 5881–5895. https://doi.org/10.1093/jxb/erv299 PMID: 26113193

86. Wang L-F, Wang M, Zhang Y. Effects of powdery mildew infection on chloroplast and mitochondrial functions in rubber tree. Tropical Plant Pathol. 2014; 39: 242–250.

87. Rodriguez-Moreno L, Pineda M, Soukupova J, Macho AP, Beuzon CR, Baron M, et al. Early detection of bean infection by Pseudomonas syringae in asymptomatic leaf areas using chlorophyll fluorescence imaging. Photosynth Res. 2008; 96: 27–35. https://doi.org/10.1007/s11120-007-9278-6 PMID: 18000760

88. Aldea M, Hamilton JG, Resti JP, Zangerl AR, Berenbaum MR, Frank TD, et al. Comparison of photosynthetic damage from arthropod herbivory and pathogen infection in understory hardwood saplings. Oecologia. 2006; 149: 221–232. https://doi.org/10.1007/s00442-006-0444-x PMID: 16758220

89. Griebel T, Zeier J. Light regulation and daytime dependency of inducible plant defenses in Arabidopsis: phytochrome signaling controls systemic acquired resistance rather than local defense. Plant Physiol. 2008; 147: 790–801. https://doi.org/10.1104/pp.108.119503 PMID: 18434604

90. Kong Q, Qu N, Gao M, Zhang Z, Ding X, Yang F, et al. The MEKK1-MKK1/MKK2-MPK4 kinase cascade negatively regulates immunity mediated by a mitogen-activated protein kinase kinase kinase in Arabidopsis. Plant Cell. 2012; 24: 2225–2236. https://doi.org/10.1105/tpc.112.097253 PMID: 22643122

91. Su SH, Bush SM, Zaman N, Stecker K, Sussman MR, Krysan P. Deletion of a tandem gene family in Arabidopsis: increased MEKK2 abundance triggers autoimmunity when the MEKK1-MKK1/2-MPK4 signaling cascade is disrupted. Plant Cell. 2013; 25: 1895–1910. https://doi.org/10.1105/tpc.113.112102 PMID: 23695980

92. Roux ME, Rasmussen MW, Palma K, Lolle S, Regue AM, Bethke G, et al. The mRNA decay factor PAT1 functions in a pathway including MAP kinase 4 and immune receptor SUMM2. EMBO J. 2015; 34: 593–608. https://doi.org/10.15252/embj.201488645 PMID: 25603932

93. Zhang Z, Liu Y, Huang H, Gao M, Wu D, Kong Q, et al. The NLR protein SUMM2 senses the disruption of an immune signaling MAP kinase cascade via CRCK3. EMBO Rep. 2017; 18: 292–302. https://doi.org/10.15252/embr.201642704 PMID: 27986791

94. Yamada K, Yamaguchi K, Shirakawa T, Nakagami H, Mine A, Ishikawa K, et al. The Arabidopsis CERK1-associated kinase PBL27 connects chitin perception to MAPK activation. EMBO J. 2016; 35: 2468–2483. https://doi.org/10.15252/embj.201694248 PMID: 27679653

95. Wang C, Wang G, Zhang C, Zhu P, Dai H, Yu N, et al. OsCERK1-mediated chitin perception and immune signaling requires receptor-like cytoplasmic kinase 185 to activate an MAPK cascade in rice. Mol Plant. 2017; 10: 619–633. https://doi.org/10.1016/j.molp.2017.01.006 PMID: 28111288

96. Coley PD, Bryant JP, Chapin FS 3rd. Resource availability and plant antiherbivore defense. Science. 1985; 230: 895–899. https://doi.org/10.1126/science.230.4728.895 PMID: 17739203

97. Huot B, Yao J, Montgomery BL, He SY. Growth-defense tradeoffs in plants: a balancing act to optimize fitness. Mol Plant. 2014; 7: 1267–1287. https://doi.org/10.1093/mp/ssu049 PMID: 24777989

98. Smakowska E, Kong J, Busch W, Belkhadir Y. Organ-specific regulation of growth-defense tradeoffs by plants. Curr Opin Plant Biol. 2016; 29: 129–137. https://doi.org/10.1016/j.pbi.2015.12.005 PMID: 26802804

99. Karasov T, Chae E, Herman J, Bergelson J. Mechanisms to mitigate the tradeoff between growth and defense. Plant Cell. 2017; 29: 666–680. https://doi.org/10.1105/tpc.16.00931 PMID: 28320784

100. Xu J, Zhang S. Mitogen-activated protein kinase cascades in signaling plant growth and development. Trends Plant Sci. 2015; 20: 56–64. https://doi.org/10.1016/j.tplants.2014.10.001 PMID: 25457109

101. Wang H, Ngwenyama N, Liu Y, Walker JC, Zhang S. Stomatal development and patterning are regulated by environmentally responsive mitogen-activated protein kinases in Arabidopsis. Plant Cell. 2007; 19: 63–73. https://doi.org/10.1105/tpc.106.048298 PMID: 17259259

102. Fillat MF, Borrias WE, Weisbeek PJ. Isolation and overexpression in Escherichia coli of the flavodoxin gene from Anabaena PCC 7119. Biochem J. 1991; 280 (Pt 1): 187–191.

103. Okazaki K, Kabeya Y, Suzuki K, Mori T, Ichikawa T, Matsui M, et al. The PLASTID DIVISION1 and 2 components of the chloroplast division machinery determine the rate of chloroplast division in land plant cell differentiation. Plant Cell. 2009; 21: 1769–1780. https://doi.org/10.1105/tpc.109.067785 PMID: 19567705

104. Fu ZQ, Yan S, Saleh A, Wang W, Ruble J, Oka N, et al. NPR3 and NPR4 are receptors for the immune signal salicylic acid in plants. Nature. 2012; 486: 228–232. https://doi.org/10.1038/nature11162 PMID: 22699612

105. Johansson ON, Nilsson AK, Gustavsson MB, Backhaus T, Andersson MX, Ellerstrom M. A quick and robust method for quantification of the hypersensitive response in plants. Peer J. 2015; 3: e1469. https://doi.org/10.7717/peerj.1469 PMID: 26734506

106. Jarvi S, Suorsa M, Paakkarinen V, Aro EM. Optimized native gel systems for separation of thylakoid protein complexes: novel super- and mega-complexes. Biochem J. 2011; 439: 207–214. https://doi.org/10.1042/BJ20102155 PMID: 21707535